Title
Particle tracer transport in a sloping soil lysimeter under periodic, steady state conditions

Authors
Wang, Chaozi
McNew, Coy P
Lyon, Steve W
et al.

Publication Date
2019-02-01

DOI
10.1016/j.jhydrol.2018.11.050

Peer reviewed

Journal of Hydrology 569 (2019) 61–76

Contents lists available at ScienceDirect

Journal of Hydrology

journal homepage: www.elsevier.com/locate/jhydrol

Research papers

Particle tracer transport in a sloping soil lysimeter under periodic, steady state conditions

Chaozi Wang[a,b], Coy P. McNew[b], Steve W. Lyon[c], M. Todd Walter[d], Till H.M. Volkman[e], Nathan Abramson[e], Aditi Sengupta[e], Yadi Wang[e], Antonio Alves Meira Neto[e], Luke Pangle[f], Peter A. Troch[e,g], Minseok Kim[h], Ciaran Harman[h], Helen E. Dahlke[b,*]

[a] College of Water Resources and Civil Engineering, China Agricultural University, Beijing 100083, China
[b] Department of Land, Air, and Water Resources, UC Davis, Davis, CA 95616, USA
[c] Department of Physical Geography, Stockholm University, SE-106 91 Stockholm, Sweden
[d] Department of Biological and Environmental Engineering, Cornell University, Ithaca, NY 14853, USA
[e] Landscape Evolution Observatory, Biosphere2, University of Arizona, Oracle, AZ 85739, USA
[f] Department of Geosciences, Georgia State University, Atlanta, GA 30303, USA
[g] Department of Hydrology and Water Resources, University of Arizona, Tucson, AZ 85721, USA
[h] Department of Geography and Environmental Engineering, Johns Hopkins University, Baltimore, MD 21218, USA

ARTICLE INFO

This manuscript was handled by Peter K. Kitanidis, Editor-in-Chief, with the assistance of Jian Luo, Associate Editor

Keywords:
Colloid
Transport
Vadose zone
Tracer
Transient
Unsaturated

ABSTRACT

Colloid transport through complex and dynamic (i.e. non-steady-state) hydrologic systems is rarely studied, owing to the difficulty of constraining initial and boundary conditions and quantifying colloid-porous media and colloid-colloid interactions in transient flow systems. Here we present a particle tracer experiment conducted on a sloped lysimeter receiving periodic rainfall events for 10 days. Four unique, DNA-labelled particle tracers were injected both in sequence and in parallel, together with a conservative tracer (deuterium), over the course of the first day and allowed to move through the system. Discharge-particle tracer concentration curves and the spatial distribution of particle tracer mass retained in the soil at the end of the experiment were found to be highly dependent on the timing of the tracer injection and the precipitation input and subsequent dynamic response of the water table. Overall, neglecting the total DLT recovery rate, the DLT particle tracer breakthrough trend (DNA-labelled particle tracer 4) was similar to deuterium and decreased over time with the exception of a few peaks later in the experiment. The individual particle tracer breakthrough curves suggest a complex system with different fast transport mechanisms (e.g. capillary barrier and size exclusion effect) and slow retention-release mechanisms (e.g. straining, physical-chemical adsorption), which resulted in particle tracers transferring faster than deuterium in the first 10 h of the experiment but being exceeded by deuterium soon after deuterium started to break through. The experiment not only highlights the interaction of repeated colloidal pollution events in hydrologic systems with different pre-event saturation conditions, but also the benefits of using multiple synchronous or sequential tracer applications to dissect explicit formulations of water flow and colloid transport processes in complex and dynamic hydrological systems. Such explicit process formulations could help improve understanding hydrologically-controlled transport through catchments and the quantitative prediction of these processes with water quality models.

1. Introduction

Many pollutants (organic, inorganic and microbial) exist in the environment as colloids whose size falls in the range between 1 nm and 10 μm (Chrysikopoulos and Sim, 1996; Sirivithayapakorn and Keller, 2003a; Smith et al., 2007; Vasiliadou and Chrysikopoulos, 2011; Wan and Wilson, 1994b; Wang et al., 2018). Colloids have a high sorptive capacity and have been shown to facilitate transport of many contaminants through the vadose zone to streams or groundwater including heavy metals, pesticides, herbicides and other pollutants that

* Corresponding author.
E-mail addresses: czwang@ucdavis.edu (C. Wang), cpmcnew@ucdavis.edu (C.P. McNew), steve.lyon@su.se (S.W. Lyon), mtw5@cornell.edu (M.T. Walter), tillv@email.arizona.edu (T.H.M. Volkman), nabramso@email.arizona.edu (N. Abramson), asengupta@email.arizona.edu (A. Sengupta), lpangle@gsu.edu (L. Pangle), patroch@email.arizona.edu (P.A. Troch), charman1@jhu.edu (C. Harman), hdahlke@ucdavis.edu (H.E. Dahlke).

https://doi.org/10.1016/j.jhydrol.2018.11.050
Received 3 June 2018; Received in revised form 6 November 2018; Accepted 16 November 2018
Available online 02 December 2018

can adsorb onto and move with colloids (Artinger et al., 2002; Barton and Karathanasis, 2003; de Jonge et al., 2004; Mills et al., 1991; Ouyang et al., 1996; Severino et al., 2007). Knowledge of the processes that control colloid transport and fate under complex, environmentally relevant conditions is required to effectively predict, manage and remediate environmental pollutants in soil and water systems. However, the sources of and pathways that colloidal pollutants take in the environment are often unknown, because of the complexity of natural soil and water systems and the legacy of accumulated pollutants already present in our environment (Zhang et al., 2015; Zhang et al., 2016). This variability in initial conditions and dynamic responses under variable system states precludes simple solutions for tracking, representing and predicting the movement of colloids in real-world systems. In order to isolate and identify the physico-chemical processes involved in colloid transport through porous media, previous studies have mainly conducted soil column experiments that investigate one or very few transport phenomena under controlled (e.g. steady-state) saturated or unsaturated conditions (Kretzschmar et al., 1999; McCarthy et al., 2002; Mishurov et al., 2008; Zhang et al., 2010). Retention profiles and breakthrough curves from these experiments are often used in particle transport models to describe how colloids are transported through the soil (e.g. advection and dispersion) and how they interact with themselves and the porous media (attachment, particle aggregation, deposition, remobilization, straining, etc.) (Bradford et al., 2003; Bradford and Torkzaban, 2008; Bradford et al., 2009; Elimelech et al., 2013). However, most of these models to date are not able to explicitly consider the physico-chemical properties of the particles, nor those of the system (Goldberg et al., 2017), which largely limits their applicability to predict colloid transport in complex, heterogeneous, non-steady state systems. Hence, in order to improve predictive tools that can capture the process dynamics of real-world systems, we need experiments that provide deeper understanding of the transport behavior of colloids and their interaction with other colloids, the fluid and the porous media under complex, environmentally relevant conditions.

Through extensive, controlled laboratory studies and systematic research, many of the physical and chemical processes affecting colloid transport in saturated and unsaturated porous media have been identified (McDowell-Boyer et al., 1986; Yao et al., 1971). In saturated porous media colloid transport is, similarly to solute transport, largely controlled by advection, dispersion, diffusion and sorption (Bradford et al., 2002). Among these processes sorption and desorption are assumed to be of primary importance in colloid transport through saturated porous media (Bradford et al., 2002). Experimental studies have also shown that colloid transport in porous media is highly dependent on the colloid size and soil grain size distribution (Auset and Keller, 2006; Mackley and Sherman, 1992; Sang et al., 2013), whereby smaller particles tend to be removed (i.e. attached to porous media) more efficiently by diffusive transport and larger particles tend to be removed more efficiently by sedimentation and interception (Yao et al., 1971).

In unsaturated porous media, the presence of air, capillary forces, pore size and the thickness of the water film around soil grains all have fundamental impacts on the retention of colloids. Colloid transport and retention in unsaturated porous media are mainly controlled by colloid adsorption (i.e. attachment, detachment) to solid-water interfaces (SWI) and air-water interfaces (AWI) (Auset et al., 2005; Gómez Suárez et al., 1999; Keller and Auset, 2007; Lazouskaya and Jin, 2008; Lazouskaya et al., 2006; Lazouskaya et al., 2013; Sang et al., 2013; Sirivithayapakorn and Keller, 2003b; Wan and Wilson, 1994a; Wan and Wilson, 1994b), straining (Bradford et al., 2003; Bradford et al., 2002; McDowell-Boyer et al., 1986), and film straining (when the water film enveloping the solid phase is not thick enough to submerge the particle) (Bradford and Torkzaban, 2008; Crist et al., 2004; Lazouskaya et al., 2013). These processes in unsaturated porous media are further complicated when the water content changes, which often means that suspended particles move closer to SWI(s) or AWI or both, leading to increased straining and physical-chemical adsorption (Bradford and Torkzaban, 2008).

In contrast to steady-state flow systems, transient hydrologic conditions such as those created by pulsed water applications (e.g. wetting-drying cycles, fluctuating water tables), often create systems consisting of both an unsaturated and a saturated zone that combine many of the processes mentioned above. Transient flow is able to mobilize more colloids, because the variation in soil water content (e.g. during infiltration or drainage) can lead to sudden changes in the local soil water potential, pore water saturation, AWI surface area, AWI locations, and thickness of water films (Zhuang et al., 2007). As such, the dynamic nature of non-steady state flow can cause shifts in chemical factors (e.g. ionic strength, pH, surface charge, chemical composition of the pore water) and physical factors (e.g. pore size distribution, shrinking and swelling of the soil) in the porous media, which might fundamentally influence the importance and magnitude of some of the processes assumed to be primary controls on colloid transport in steady-state flow systems. However, further insights into these processes and their potential interactions can only be explored through complex, dynamic, non-steady state experiments.

Among the considerable number of studies of colloid transport in saturated or unsaturated porous media, very few have conducted larger-scale (e.g. lysimeter) experiments with transient flow conditions (see Table S1, supplementary material). Predelus et al. (2005) studied colloidal nanoparticle transport in a 1.6 m^3 unsaturated lysimeter comprised of two soil layers, to determine the effect of capillary barriers and preferential flow on colloid transport. However, they used silica nanoparticles with a diameter of 50–60 nm, which were much smaller in comparison to the fine sand (0–0.2 cm) and gravel (0.4–1.1 cm) porous media used in the experiment. In addition, they only applied one continuous rainfall event over the entire experiment, and their experiment was under steady-state flow conditions.

The objective of our experiment was to explore the potential for interactions between multiple synchronous and sequential particle tracer injections in a large, sloping and variably saturated-unsaturated system under transient hydrologic conditions (periodic irrigation). As such, we are attempting to capture a scenario more realistically analogous to (perhaps repeated) colloidal pollutant spills in the environment. For this purpose, a 10-day experiment was conducted using a 1 m^3 sloped lysimeter (the “miniLEO”) at the Landscape Evolution Observatory (LEO) at the University of Arizona to estimate the fate and transport of four synchronous and sequentially injected DNA-labelled particle tracers and one conservative tracer (deuterium). The DNA-labelled particles used in this experiment are a new tracer technology invented by Sharma et al. (2012), which, because of the use of synthetic DNA sequences, effectively provides an unlimited number of uniquely identifiable tracers with identical transport properties. The tracers consist of short single-stranded DNA encapsulated by polylactic acid (PLA) microspheres (Dahlke et al., 2015; McNew et al., 2018; Sharma et al., 2012).

2. Methods

2.1. Experimental setup

2.1.1. The miniLEO sloped lysimeter

A 10-day controlled experiment was conducted at the Landscape Evolution Observatory within the Biosphere 2 indoor laboratory, University of Arizona, USA (Pangle et al., 2015), using a sloped lysimeter (the miniLEO) with an inner length of 200 cm, inner width of 50 cm, inner depth of 100 cm, and a bed slope of 10 degrees (Fig. 1). The sloped lysimeter is intended to be a prototype segment of a hillslope, a basic building-block of a watershed (Kim et al., 2016; Pangle et al., 2015). The lysimeter had no flow boundaries on the upslope and length sides, while the downslope side was screened with perforated plastic (14% porosity and 2 mm diameter pores) supported by steel bars (Fig. 1b). Discharge was collected from the lysimeter in a trough at the

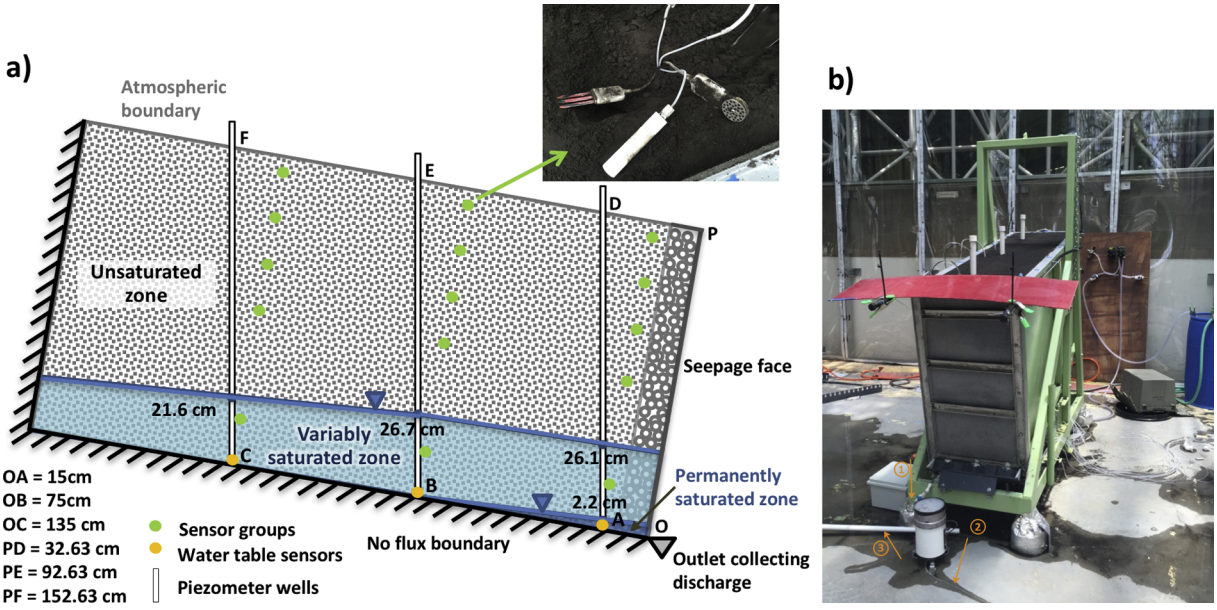

Fig. 1. Sketch (a) and photograph (b) of the experimental setup. Boundary conditions are indicated by the color of the boundary (a). The two dark blue lines and the corresponding triangles indicate the location of the lowest and highest water table (a). The lysimeter was divided into three hydrologic zones (a): a permanently unsaturated zone (white fill), a variably saturated zone (light blue fill), and a permanently saturated zone (dark blue fill). The seepage face and the trough collecting discharge are shown in the photograph (b). (For interpretation of the references to color in this figure legend, the reader is referred to the web version of this article.)

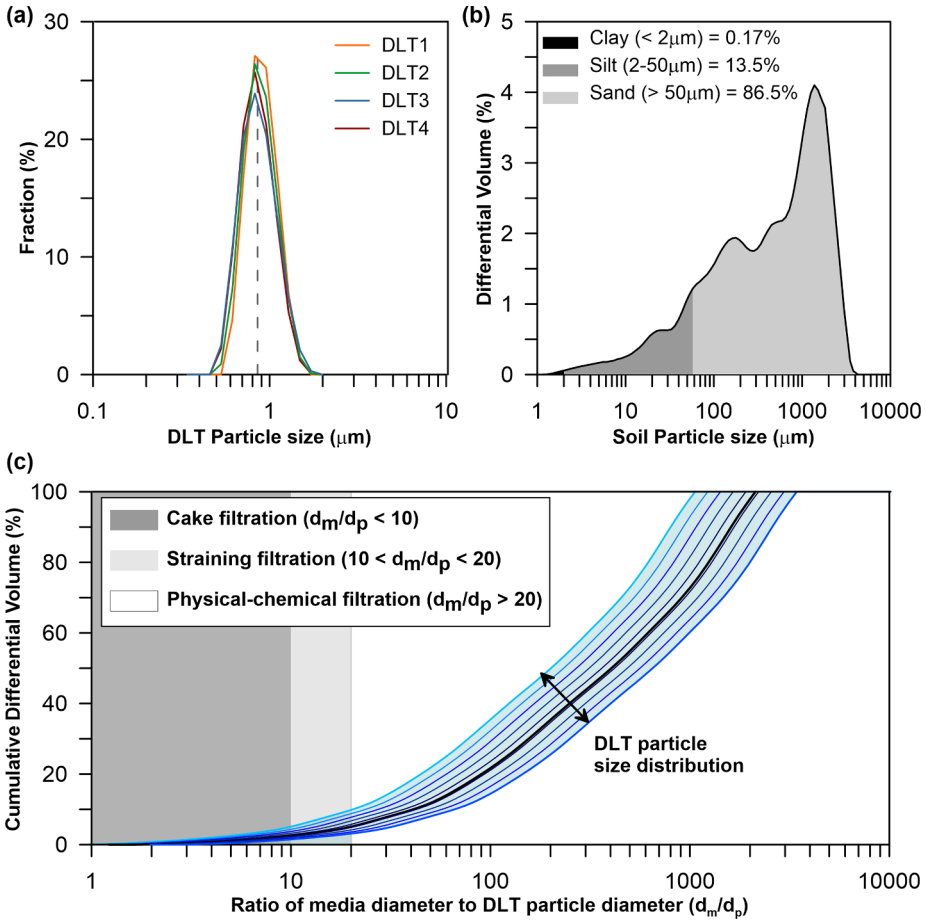

Fig. 2. Particle size distributions for each of the four DLTs (a), and the porous media (b). Plot of the ratio of porous media diameter to DLT particle diameter (d_m/d_p) for each DLT size bin (blue and black lines) to the cumulative differential volume (%) of the porous media (c). Shaded areas show filtration mechanisms defined by McDowell-Boyer et al (1986) based on the observed d_m/d_p ratios. (For interpretation of the references to color in this figure legend, the reader is referred to the web version of this article.)

bottom of the downslope seepage face (Fig. 1). The lysimeter was packed with 0.05 m^3 of gravel and 0.95 m^3 loamy sand: 33 cm of wet soil were filled into the lysimeter and compacted to a homogeneous layer of 25 cm thickness with a tamping device. This procedure was repeated 4 times to achieve a total of 1 m homogeneous soil. The gravel was placed in a 10 cm thick layer along the downstream face of the lysimeter to mimic the flow conditions in the larger experimental hillslope at the LEO (please see Pangle et al. (2015) Fig. 2 for photographs of LEO setup).

The lysimeter was packed with crushed, late Pleistocene basaltic tephra extracted from near Merriam Crater in northern Arizona, USA (Pangle et al., 2015). The porous media was of a loamy sand texture with 86.5% sand (> 50 μm), 13.5% silt (2–50 μm) and 0.17% clay (< 2 μm) (by volume); the particle size distribution is shown in Fig. 2(b). The specific surface area of the porous media was 0.92 m^2/g, porosity was 0.47, bulk density was 1.48 g/cm^3, particle density was 2.66 g/cm^3, and saturated hydraulic conductivity was 12.1 m/d (1.4×10^{-4} m/s) (Gevaert et al., 2014; Kim et al., 2016; Pangle et al., 2015; Pohlmann et al., 2016; van Haren et al., 2017; Veevaert, 2012). Mineralogically, the porous media was composed of basaltic glass 57.8%, labradorite (feldspar) 23.4%, forsterite (olivine) 12.6%, diopside (pyroxene) 5.3%, and titanomagnetite 1.0% (by weight) (Pangle et al., 2015; Pohlmann et al., 2016). The gravel consisted of the same mineral composition, but had a much larger grain size (~1 cm diameter). The zeta potential of the porous media was −37.8 mV, measured with an electrokinetic analyzer (SurPASS, Anton Paar, Graz, Austria).

2.1.2. Lysimeter instrumentation

A suite of hydrologic sensors was installed within the lysimeter following the same design described in Kim et al. (2016). A magnetic flow meter (Seametrics PE102) was used to continuously measure the amount of water applied by four sprinklers onto the surface of the lysimeter and its surrounding area. The spatial distribution of the rainfall was measured *a priori* with cups collecting rainfall in a 10 × 3 grid to determine the actual amount of water that was falling onto the surface of the soil lysimeter. Real-time discharge was measured with a tipping bucket gauge (Onset RG3) at the outlet of the soil lysimeter. The lysimeter rested on four load cells (one at each corner) that measured the weight of the soil box; the weight was used to calculate the change in water storage in the system. A total of 15 water potential sensors (MPS-2), 15 soil pore water samplers (Prenart Super Quartz sampler) and 15 volumetric water content and temperature sensors (Decagon 5TM sensor) were installed at three slope positions (downslope, midslope and upslope) and five depths (5, 20, 35, 50 and 85 cm) as shown in Fig. 1a. The dynamic water table was measured with two Campbell CS451 pressure transducers and one HOBO water level logger at the downslope, midslope and upslope position within the lysimeter (at 15, 75 and 135 cm distance from downslope face, Fig. 1a). The sampling frequency of all hydrologic sensors was 1 min.

2.1.3. Periodic steady state condition

The lysimeter was packed 35 days before the start of the 10-day experiment, which started on June 14, 2016. Rainwater was applied starting 5 days prior to the experiment to prime the system. Periodic steady state conditions were created in the system by applying an identical rainfall sequence each day. For the initiation and duration of the experiment, three rainfall pulses of 2-h duration with a rainfall intensity of 30 mm h^{-1} were applied each day: the first pulse was applied from 8:00 to 10:00, the second pulse from 12:00 to 14:00, and the third pulse from 16:00 to 18:00. The periodic steady state regime was used to study colloid transport in transient flow and the influence of different stages of the wetting-drying cycle on colloid transport.

2.1.4. Tracer application

Five tracers were applied to the lysimeter, consisting of one

Table 1
Summary of the physico-chemical properties and application timing of the DNA-labelled particle tracers.

	Number of nucleotides	Tracer size (diameter in nm)	Zeta potential (mV)	Tracer solution	Application duration
DLT1	87	886	−37	2 batches in 550 ml water	Day 1: 8:00 – 10:00 (1st rainfall pulse)
DLT2	90	897	−36	2 batches in 550 ml water	Day 1: 12:00 – 14:00 (2nd rainfall pulse)
DLT3	90	894	−37	2 batches in 550 ml water	Day 1: 16:00 – 18:00 (3rd rainfall pulse)
DLT4	98	856	−35	2 batches in 1500 ml water	Day 1: 8:00 – 10:00, 12:00 to 14:00, 16:00 to 18:00; during all three rainfall pulses

conservative tracer (deuterium, D) and four DNA-labelled particle tracers. We adopted four DNA nucleotide sequences (T3M, T4M, T10, T11) from Dahlke et al. (2015) to create four DNA-labelled particle tracers (DLTs) named DLT1, DLT2, DLT3 and DLT4 (please see Table 1 for the number of nucleotides of each DLT and Table S2 in supplementary materials for the exact sequences). The average tracer sizes and zeta potentials are provided in Table 1, and particle size distribution of each kind of DLT is provided in Fig. 2a. More information on the fabrication and extraction of DLTs from water and soil samples is provided in the Supplementary materials (S1–S4).

The D and one of the DLTs (DLT4) were applied during all three rainfall pulses on the first day of the experiment. D was applied with the rainwater; all DLTs were applied manually with spray bottles on the soil surface in a spatially and temporally uniform manner. While DLT4 was applied during all three rainfall pulses, DLT1 was applied only during the first rainfall pulse, DLT2 only during the second, and DLT3 only during the third rainfall pulse on day 1 (Table 1). The baseline δD value of rain water was −57‰ (all isotopic data are reported relative to Vienna Standard Mean Ocean Water, equivalent to 1.5395×10^{-2} mmole/ml HDO), and the δD value of labeled rain water was 765‰ (equivalent to 2.8810×10^{-2} mmole/ml HDO). For each DLT, two batches of concentrated tracer were mixed with ultrapure water. For DLT1, DLT2, and DLT3 the concentrated DLT was mixed with 550 ml of water, while for DLT 4 the concentrated DLT was mixed with 1500 ml of water to provide enough volume for three 2-h application. In this way, the comparison between the breakthrough curve of D and the breakthrough curve of DLT4 could be used to understand how the behavior of the DLTs was different from a conservative tracer, as they were applied during the same periods. And the comparison between the superimposed breakthrough curve of DLT1-3 and breakthrough curve of DLT4 could be used to understand if different stages of the wetting-drying cycle or other factors would influence the behavior of the DLTs.

2.2. Breakthrough and retention sampling and analysis

The discharge collected in the trough at the bottom of the downslope face of the lysimeter was split three ways. One tube with a control valve allowed manual sampling of discharge from the main line (Fig. 1b, arrow ①). When the control valve was closed, all the discharge was routed to a tipping bucket to measure discharge after which it was split two ways. One tube directed the outflow from the tipping bucket gauge to an autosampler (customized with a single channel peristaltic pump and a stepper motor (Adafruit Industries) controlled by an Arduino Uno microcontroller board (Kim et al., 2016) (Fig. 1b, arrow ②). Another tube diverted the discharge to a Los Gatos Research DLT-100 Laser for real-time D measurements (δD relative to Vienna Standard Mean Ocean Water) (Kim et al., 2016) (Fig. 1b, arrow ③). Manual samples were taken every half hour during the daytime on the first three days of the experiment (8:00–20:00). Automatic samples were taken every half hour during the first three days and every hour for the remainder of the experiment. Discharge samples were taken using sterilized 5 ml tubes (Eppendorf AG, Hamburg, Germany).

After the 10th day of the experiment, the lysimeter was excavated and soil samples were taken to estimate the tracer mass retained in the porous media. For this, the lysimeter was divided into 18 zones (white grid shown in Fig. 7), and one sample (about 500 g of soil) was taken from each of the 18 zones after thorough mixing of all the soil in that zone.

Detailed methods of extraction and quantification of the four DLTs in each collected soil and discharge sample are described in the Supplementary materials S2–S5 and McNew et al. (2018).

2.3. Tracer recovery and retention analysis

For D, the input mass was known (the D tracer input concentration was multiplied by the corresponding input rainfall amount), and both discharge concentration and discharge were measured at the frequency of one value per minute. The normalized cumulative transferred (i.e., recovered) mass could simply be calculated by:

$$M_D(t_m) = \frac{\int_0^{t_m} C(t)Q(t)dt}{M_{in\_D}} \quad (1)$$

where t is time (min), M_D is normalized cumulative transferred mass, t_m represents the sampling time the M_D is calculated for ($m = 0, 1, 2,\ldots, n$; $t_0 = 0$, $t_n = 14400$) (min), M_{in_D} is the total input D mass, $C(t)$ is the discharge concentration of D at time t (mmole/ml), $Q(t)$ is discharge at time t (ml/min).

Note, that we first converted the concentration unit from per mil to mmole/ml, and then subtracted the background concentration from each concentration value. The background concentration was taken as the mean concentration of the first 4 h of the experiment. Observed values less than the background value were set to zero.

The discharge concentration data for other tracers were measured at the frequency of one data point every half hour or one hour; while discharge was measured at the frequency of one value per minute. Moreover, because the fabrication, application and analysis procedure of the DLTs caused unquantifiable losses in tracer mass, the total DLT input mass was estimated as the sum of the DLT mass retained in the soil at the end of the experiment and the DLT mass recovered from the discharge. The unknown losses, for example, included 1) the unencapsulated DNA strands that were washed off together with fabrication reagents during the washing step in the fabrication (Supplementary materials S1), 2) the DLTs that did not resuspend well due to aggregation, 3) spray sometimes reached beyond the lysimeter boundaries, and 4) the DNA strands that were not effectively extracted from the polymer microspheres in the collected discharge and soil samples (the extraction efficiency was not 100%, although over 90%, please see McNew et al., 2018 for more details). Therefore, the calculation of the normalized cumulative transferred DLT mass was more complicated.

The total discharged mass was:

$$TDM = C_i(t_1)\int_0^{\frac{t_1+t_2}{2}} Q(t)dt + \sum_{j=2}^{n-1} C_i(t_j)\int_{\frac{t_j+t_{j-1}}{2}}^{\frac{t_j+t_{j+1}}{2}} Q(t)dt + C_i(t_n)\int_{\frac{t_n+t_{n-1}}{2}}^{t_n} Q(t)dt \quad (2)$$

where t is time (min), t_j represents each sampling time ($j = 0, 1, 2,\ldots,$ n; $t_0 = 0$, $t_n = 14400$), TDM is total discharged mass, i represents the tracer types (DLT1, DLT2, DLT3 or DLT4), $C_i(t_j)$ is the concentration of tracer i at sampling time t_j (copies/ml), $Q(t)$ is discharge at time t (ml/min).

The concentration of each DLT in each of the 18 excavated soil zones were interpolated and plotted. The total number of copies of each DLT retained in each of the 18 soil zones was estimated by multiplying the total mass of soil in that zone and the concentration of each DLT in that zone. Therefore, the total input mass for each DLT was calculated by:

$$W_i = TDM + \sum_{k=1}^{k=18} N_{i,k} \quad (3)$$

where W is total input mass (copies), and the summation item is the total retained mass in soil profile, $N_{i,k}$ is the mass of tracer i in soil zone k ($k = 1, 2, \ldots, 18$).

Normalized cumulative transferred mass was calculated for each tracer at each discharge sampling time by summing up the product of concentration and discharge over time and dividing by the total input mass:

$$M_i(t_m) = \frac{C_i(t_1)\int_0^{\frac{t_1+t_2}{2}} Q(t)dt + \sum_{j=2}^{m-1} C_i(t_j)\int_{\frac{t_j+t_{j-1}}{2}}^{\frac{t_j+t_{j+1}}{2}} Q(t)dt + C_i(t_m)\int_{\frac{t_m+t_{m-1}}{2}}^{t_m} Q(t)dt}{W_i} \quad (4)$$

where M is normalized cumulative transferred (i.e., recovered) mass, and t_m represents the sampling time the M_i is calculated for ($m = 0, 1, 2, \ldots, n$; $t_0 = 0$, $t_n = 14400$) (min).

The normalized cumulative transferred (i.e., recovered) tracer mass reveals the arrival of each tracer at the outlet of the lysimeter and the transport pattern over time.

Normalized load curves were calculated as the product of tracer discharge concentration and discharge over a given sampling interval, and the total input mass was used to normalize each load value for that tracer:

$$L_i(t_j) = \begin{cases} \frac{C_i(t_1)\int_0^{\frac{t_1+t_2}{2}} Q(t)dt}{W_i}, (j=1) \\ \frac{C_i(t_j)\int_{\frac{t_j+t_{j-1}}{2}}^{\frac{t_j+t_{j+1}}{2}} Q(t)dt}{W_i}, (j=2,3,\cdots,n-1) \\ \frac{C_i(t_n)\int_{\frac{t_n+t_{n-1}}{2}}^{t_n} Q(t)dt}{W_i}, (j=n) \end{cases} \quad (5)$$

where $L_i(t_j)$ is the normalized load of tracer i over the j-th sampling time (copies per sampling interval).

In our transient variable system, the normalized load breakthrough curves provide information about the ability of the system to mobilize each tracer, taking total recovery rate into consideration. In addition to the normalized load and recovered tracer mass curves for each DLT and the D, we also created a superimposed curve of the three individual DLT pulses by summing the normalized cumulative transferred mass of DLT1, DLT2 and DLT3 and dividing them by 3. This superimposed cumulative curve (named superimposed DLT1-3 for the remainder of this paper) allows direct comparison with DLT4 and D, which were applied during all three rainfall pulses on day 1.

In order to better understand the hydrologic factors controlling the transport of the DLTs and the deuterium tracer within the lysimeter, peaks were identified in the hydrologic variables (storage, discharge, water level, volumetric water content) and sorted by time for each day and rainfall pulse. Hydrological time series were first smoothed to remove noise in the 1-minute-time-interval data, and then peaks of the smoothed curves were automatically identified using MATLAB code (the MATLAB code and algorithm of the smoothing and peak identification are provided in the supplementary materials). The peaks of the deuterium breakthrough curve and the normalized DLT load curves were automatically identified as well, but without pre-smoothing. Then, the peaks of the hydrological variables were sorted for each rainfall pulse and day. This detailed spatio-temporal analysis of hydrologic and tracer transport dynamics provided helpful insights for the identification of dominant transport mechanisms within the lysimeter.

2.4. Statistical analysis

The Pearson correlation coefficient, r, was calculated between the base-10 logarithm of the DLT breakthroughs and all hydrologic variables (i.e. discharge, storage, rainfall, water level, volumetric water content) and the observed deuterium breakthrough. The log-transformation of both observed DLT concentration and load was done to transform the highly positively-skewed DLT data distribution to a more normal distribution. In addition, DLT2 and DLT3 time series were shifted to the injection time of DLT1, DLT4 and D. Statistical analysis was done in MATLAB and r as well as associated p-values recorded.

3. Results

3.1. Hydrology of the system

3.1.1. Storage, discharge and water table dynamics in the system

Fig. 3 depicts the rainfall, storage, discharge and water level dynamics in the sloped lysimeter for the 10-day experiment. In response to the three rainfall pulses applied each day, the storage and discharge of the system showed three distinct peaks with sharply rising and falling limbs and longer-tailed recessions during the intervening night period. System storage varied daily between 270 (around 6:00) and 350 mm (around 19:00) in response to rainfall events. Storage responded more quickly to the first rainfall pulse each day than discharge, which only increased to 50% of the daily maximum during the first rainfall pulse, followed by a clear increase during the second and third rainfall pulse when the water table expanded in upslope direction, increasing connectivity in the hillslope. The water level in the up-, mid-, and downslope position rose to about 27 cm above the bottom in response to the third rainfall pulse each day. Overall, the water level data showed less pronounced peaks. The water level in the up- and mid-slope position frequently decreased to zero during the night period indicating drainage of this part of the hillslope during the intervening period. Only the downslope water level maintained a minimum height of 2.2 cm above the bottom of the lysimeter during the intervening period. Over the duration of the experiment, 1,759 mm of rainfall were applied (adjusted for the spatial rain distribution of the sprinklers); the total discharge was 1,721 mm, resulting in a nearly closed water balance (2.2% loss). The applied rainfall amount per day (180 mm/day) is large compared to the storage of the system. However, the upper 75% of the system remained unsaturated during the experiment, which means that the rainfall rate was not unreasonably large. The large rainfall rate was used to speed up the experiment; otherwise, the experiment would have taken a much longer time.

Fig. 4 shows the measured volumetric water content (VWC) at the upslope, midslope and downslope position and five different depths within the sloped lysimeter. VWCs showed the greatest amplitude in the first 20 cm of the system and a more dampened response in the lower half. With every rainfall application, VWC increased rapidly throughout the lysimeter, approaching saturation in some locations (e.g. at 5 and 50 cm). Both VWC sensors installed at 85 cm depth at mid-slope and downslope remained above 45% for the duration of the experiment, indicating nearly saturated conditions (e.g. capillary fringe). The downslope sensor showed a steady increase in VWC over the course of the experiment, which may have been drift in the sensor calibration, or possibly an increase in porosity (perhaps due to internal piping erosion near the outflow face). Surprisingly, the mid-slope sensor installed at 35 cm showed consistently high and less variable moisture contents, which are either an indication of sensor malfunction or the sensor might have been in an area of local low permeability and perched saturation, despite efforts to ensure a homogenous packing.

3.1.2. Definition of hydrologic and tracer transport zones

Based on the measured water table at the down-, mid- and upslope position, the lysimeter was divided into three hydrologic zones: i) a permanently unsaturated zone, ii) a transient, variably saturated zone, and iii) a permanently saturated zone (Fig. 1a). About 0.5% of the system was permanently saturated and maintained a minimum water table of about 2.2 cm above the bottom of the lysimeter (Fig. 1a, dark blue area). During rainfall events, the water table rose to about 20–27 cm above the bottom of the lysimeter, creating a transient and variably saturated zone (22.53% of the total system; Fig. 1a, light blue area), above which the porous media was permanently unsaturated (76.97% of the total system; Fig. 1a, white area). These zone definitions will be used for the remainder of this paper to discuss different flow and

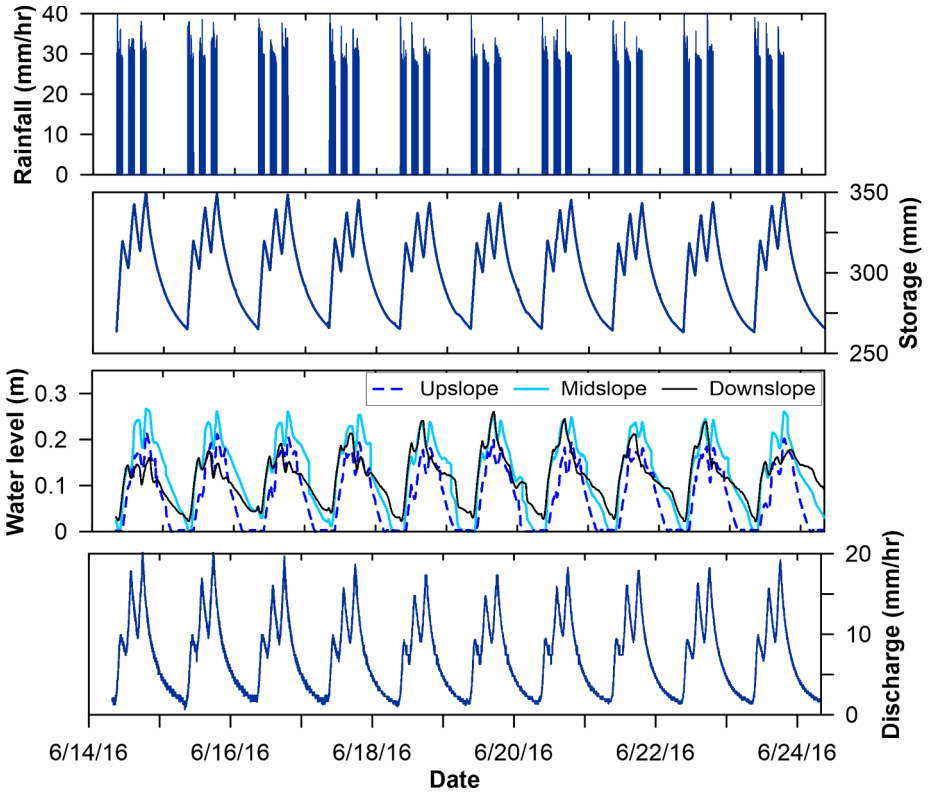

Fig. 3. Time series of major hydrologic variables for the 10-day experiment.

transport mechanisms in the system.

3.2. Tracer transport through the system

3.2.1. Breakthrough analysis

Table 2 shows the tracer mass recovered in discharge (uncertainty provided as the relative standard deviation of qPCR analysis for each DLT) and Fig. 5 shows the D and DLT time-concentration plots and normalized DLT loads (circle diameters) for the 10-day experiment. Compared to the 97.78% recovery of D in discharge, the majority of the DNA tracer mass was retained in the soil matrix (98–99%, Table 2). The DNA tracer mass recovered in the discharge decreased incrementally from DLT1 (1.44%, 6.35E + 10 out of 4.41E + 12) to DLT4 (1.04%, 2.67E + 10 out of 2.57E + 12), to DLT2 (0.52%, 1.54E + 10 out of 2.97E + 12) and DLT3 (0.19%, 1.71E + 10 out of 9.14E + 12) (Table 2). If the sequentially applied tracers responded to the water flow linearly, the total recovery rate of DLT1, DLT2 and DLT3 should be 3 times of the recovery rate of DLT4. However, the combined total recovery rate of DLT1, DLT2 and DLT3 (2.15%) was only 2 times of the recovered percentage of DLT4 (1.04%) (Table 2), which confirmed the non-linear response of the sequentially applied DLTs. Recall that the total input DNA copies were calculated by Eq. (5), i.e. the sum of the discharged and retained copies.

Except for a 12-h gap in the night of day 1, the majority of the applied D was advected and dispersed through the system during days 1–3 of the experiment. On day 1, the discharge maintained a baseline signal of −57‰ before the water became more enriched in D at around 16:00 on Day 1. D peaked around 18:00 on day 2 at 515‰ after which it decreased to near the background concentration around 20:00 on Day 3.

In comparison, the DLT time-concentration curves showed a more erratic behavior with sharper peaks (Fig. 5). Identical log-scale y-axes were used to plot the DLT breakthrough curves to provide better comparison between the different DLTs. The first breakthrough of all four DLT tracers occurred prior to the D tracer breakthrough, which is consistent with other observations of colloidal transport in porous media (Auset et al., 2005; Keller and Auset, 2007; Mohanram et al., 2010; Sirivithayapakorn and Keller, 2003a; Toran and Palumbo, 1992) and results of the reduced pore availability to transport these large particles (Auset et al., 2005; Mohanram et al., 2010; Sirivithayapakorn and Keller, 2003a). Most of the tracer peaks occurred early in the experiment and at times when rainfall was applied. Some smaller peaks also occurred on days 6–8 of the experiment. DLTs could not be detected in the discharge in the last 44 h of the experiment, which indicates that almost all the DLTs that could come out under the experimental condition had already come out by the end of the experiment. Comparing the 4 subfigures for the 4 DLTs, the decreasing recovery rate from DLT1 to DLT4 to DLT2 to DLT3 was clearly shown by the diameter of the circles showing loads normalized by total input mass. However, focusing on each subfigure, the highest loads for each tracer tended to be associated with the first irrigation pulse of each daily sequence. The DLT breakthrough curves did not show a consistently decreasing trend in tracer load (Fig. 5). For example, both DLT3 and DLT4 showed higher loads on day 3 of the experiment than on day 1.

The normalized cumulative transferred mass of all the tracers are shown in Fig. 6. The final transferred percentage was the recovery rate (97.78% for D, Fig. 6a; and about 1% as tabulated in Table 2 for DLTs, Fig. 6b). If the DLTs were transported in a conservative manner, the normalized cumulative mass breakthrough curves of D, DLT4 and the superimposed DLT1-3 should overlap. However, except for DLT3, which was injected during the third rainfall pulse on Day 1, all the other DLTs had mass recovery larger than D before 6/14 18:00 at the end of the third rainfall pulse on Day 1, even though the injection of DLT2 occurred later than that of D (Fig. 6b). However, D started to breakthrough around 6/14 16:00 and exceeded the DLTs within about 2 h. Among the four DLTs applied, DLT4 showed a breakthrough behavior most similar to that of D, if the total recovery rate is neglected and one only focuses on the trend of the breakthrough (comparing Fig. 6a and b). This is because DLT4 and D were both injected during each of the

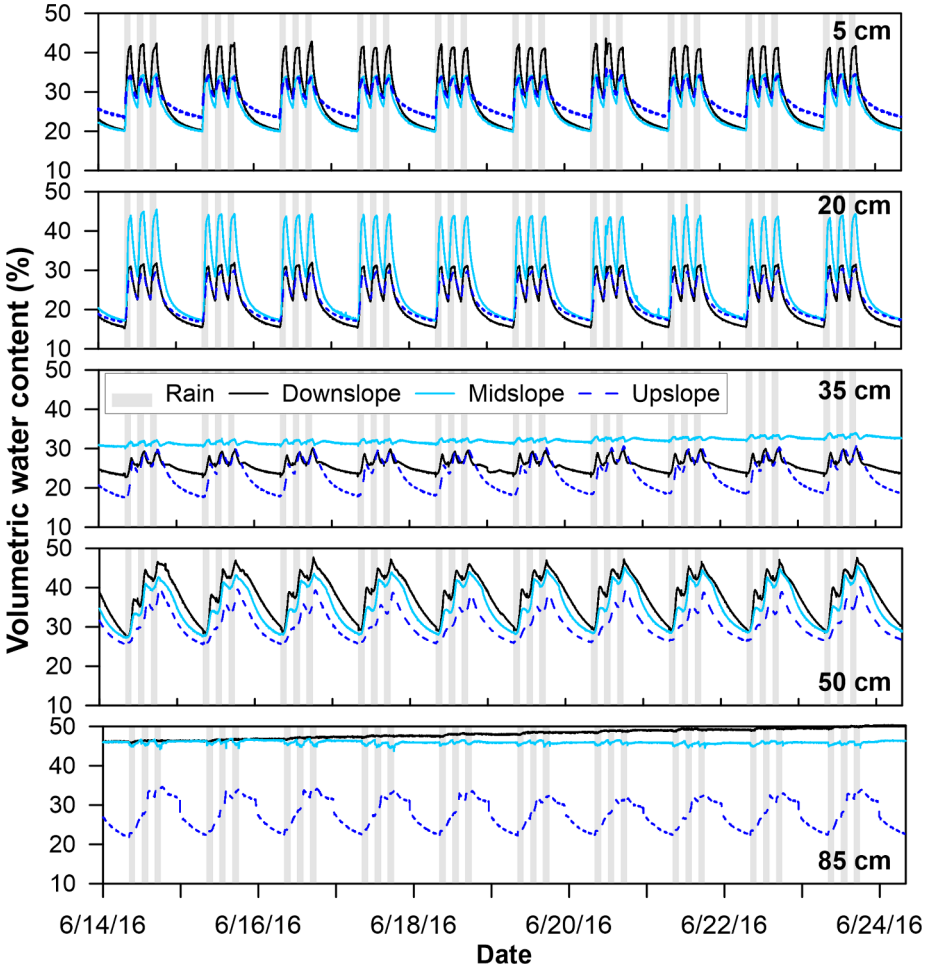

Fig. 4. Time series of the volumetric water content measured at the upslope (blue dashed line), midslope (light blue line) and downslope (black line) position at five different depths (5, 20, 35, 50, 85 cm) in the miniLeo sloped lysimeter. (For interpretation of the references to color in this figure legend, the reader is referred to the web version of this article.)

three rainfall pulses on Day 1 of the experiment. Note, that a conservative tracer moves with water without sorption to soil media and without degradation during the experimental span (Flury and Wai, 2003). Preliminary degradation experiments (data not shown) showed that the DLTs did not degrade during the experimental span (10 days). Therefore, the most likely explanation for the non-conservative breakthrough of DLTs is that they strained by and adsorbed to soil media (lower total recovery), and moved with preferential flow caused by capillary barrier and size exclusion effects (faster early breakthrough), which will be discuss in details in Section 4.1.

3.2.2. Correlation of DLTs to hydrologic variables

The Pearson correlation coefficients listed in Table 3 highlight clear relationships and hydrologic drivers for the observed DLT transport through the miniLeo hillslope. Hydrologic variables that were highly correlated to the DLT breakthrough were interpreted to be direct drivers of DLT transport. All DLTs were significantly correlated to rainfall and deuterium. To our surprise, none of the DLTs were significantly correlated to discharge, the change in storage or the water level in the mid-slope and upslope part of the hillslope. All DLTs were highly correlated to the downslope VWC at 85 cm depth; however, this might be

Table 2
Total DNA mass balance (uncertainty provided as the relative standard deviation of qPCR analysis for each DLT).

	Depth (cm)	DLT1	DLT2	DLT3	DLT4
Total input (DNA copies)		4.41 ± 0.99E+12	2.97 ± 0.54E+12	9.14 ± 2.10E+12	2.57 ± 0.61E+12
Total retained in soil (DNA copies)		4.35 ± 0.98E+12 (98.56 ± 22.21%)	2.96 ± 0.54E+12 (99.48 ± 18.05%)	9.13 ± 2.10E+12 (99.81 ± 22.91%)	2.54 ± 0.60E+12 (98.96 ± 23.47%)
Total discharge (DNA copies)		6.35 ± 1.43E+10 (1.44 ± 0.32%)	1.54 ± 0.28E+10 (0.52 ± 0.09%)	1.71 ± 0.39E+10 (0.19 ± 0.04%)	2.67 ± 0.63E+10 (1.04 ± 0.25%)
Soil zones	0–5 cm	96.40 ± 21.73%	94.85 ± 17.21%	88.01 ± 20.20%	96.44 ± 22.87%
	5–50 cm	2.16 ± 0.49%	4.62 ± 0.84%	11.60 ± 2.66%	2.48 ± 0.59%
	50–100 cm	0.00%	0.01 ± 0.00%	0.20 ± 0.05%	0.04 ± 0.01%

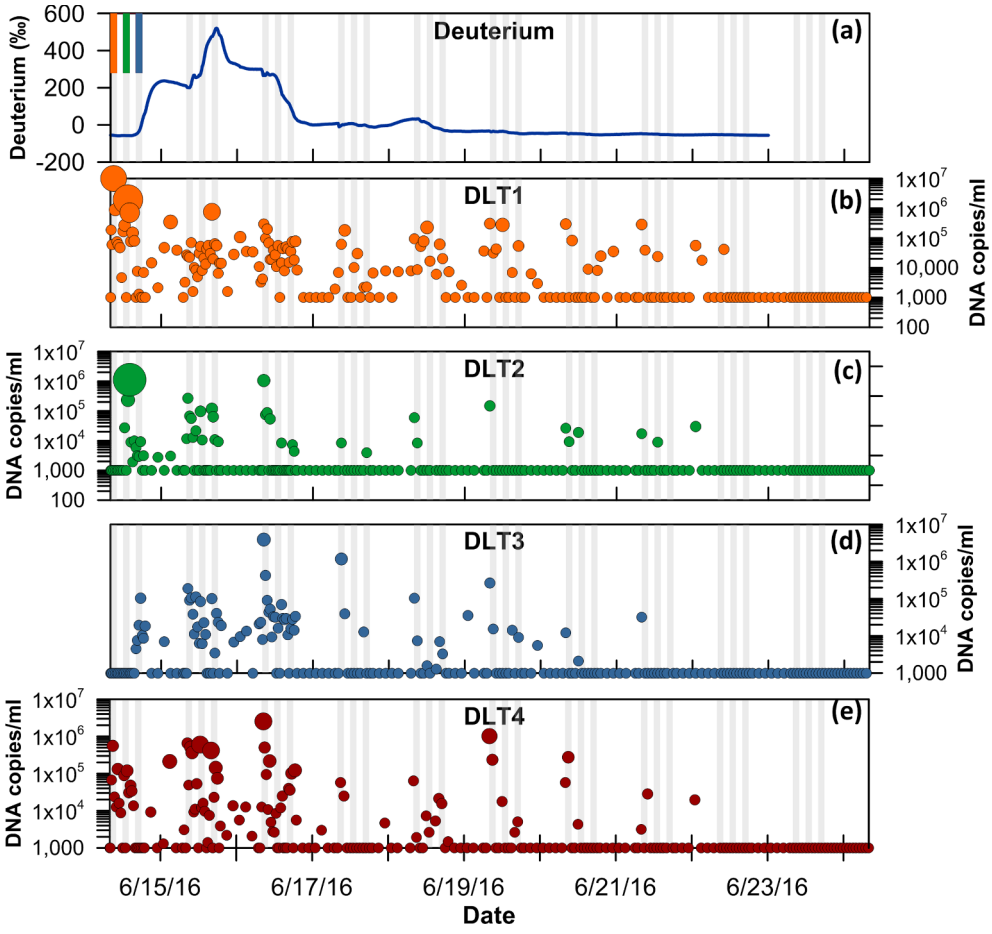

Fig. 5. Breakthrough concentrations of deuterium (a) and DNA-labelled particle tracers DLT1 (b), DLT2 (c), DLT3 (d), and DLT4 (e), for the 1 m^3 miniLeo lysimeter at the Biosphere 2 in Arizona. The detection limit of the qPCR is 1000 DNA copies per ml. Any copy number under 1000 is shown as 1000 in the figure. Note that the circle diameter indicates the tracer load normalized by the corresponding total input mass. Grey bars indicate the rainfall pulses. The colored bars in the upper left corner show the injection time of each tracer.

due to a malfunctioning sensor, as shown in Fig. 4. The observed significant correlation to the mid-slope 35 cm VWC could be an artifact of the location of the sensor and the previously described possibility of perched saturation occurring in this part of the hillslope. Most of the DLTs also showed significant correlation to the VWC at 5 and 20 cm at the downslope, mid-slope and upslope (5 cm only) position (Table 3), which could suggest that the top 5–20 cm soil was the biggest obstacle on their way to the outlet, i.e., being able to pass through the topsoil was almost sufficient to reach the outlet.

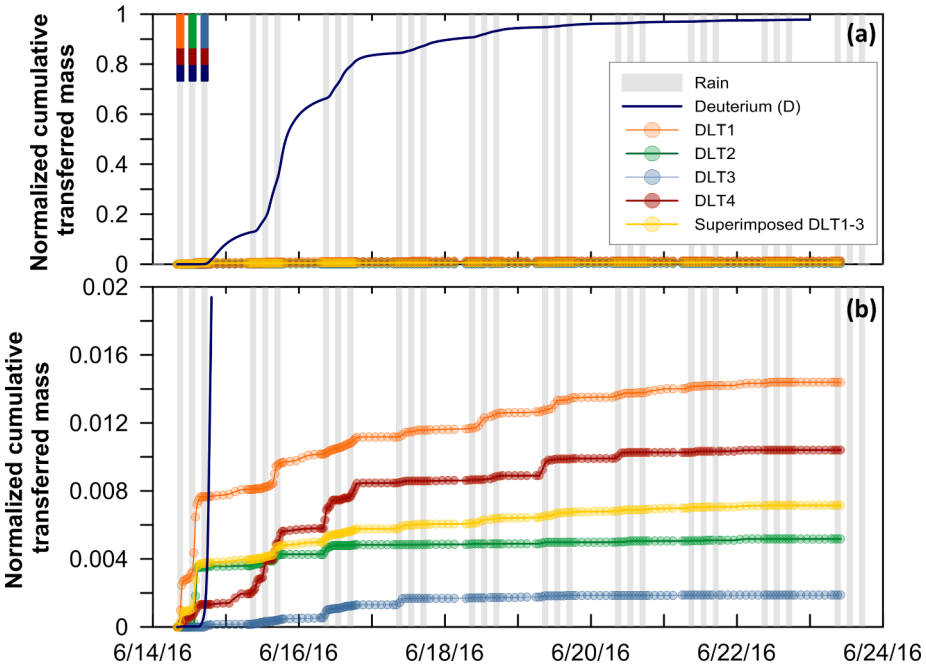

Fig. 6. Normalized cumulative curves of recovered DLT1, DLT2, DLT3, DLT4, D and superimposed DLT1-3 tracer mass. The colored bars in the upper left corner show the injection time of each tracer. Each data point was calculated by dividing the cumulative recovered mass by the total input mass. (a) shows the full range of the cumulative transferred mass, and (b) focuses on the range of the DLT cumulative transferred mass.

Table 3
Pearson correlation coefficients between tracer breakthroughs and relevant hydrologic variables. All DLT data was log-transformed prior to the analysis.

		Q	S	P	Deu-terium	Water level			Volumetric water content															
									Downslope					Mid-slope					Upslope					
						DS	MS	US	5 cm	20 cm	35 cm	50 cm	85 cm	5 cm	20 cm	35 cm	50 cm	85 cm	5 cm	20 cm	35 cm	50 cm	85 cm
DLT1	log(C)	ns	ns	**0.19***	**0.44**†	**−0.14***	ns	ns	ns	ns	ns	ns	**−0.61**†	ns	ns	**−0.49**†	**−0.14***	ns	ns	ns	ns	ns	ns	ns
	log(Load)	ns	ns	**0.16***	**0.46**†	ns	ns	ns	**0.15***	**0.15***	ns	ns	**−0.61**†	ns	**0.15***	**−0.49**†	ns	ns	ns	ns	ns	ns	ns	ns
DLT2	log(C)	ns	ns	**0.45**†	**0.21****	**−0.22****	ns	ns	**0.20****	**0.16***	ns	**0.16***	**−0.36**†	**0.19***	**0.15***	**−0.18***	ns	**−0.22****	**0.16***	ns	ns	ns	ns
	log(Load)	ns	ns	**0.44**†	**0.21****	**−0.18***	ns	ns	**0.22****	**0.19***	ns	ns	**−0.36**†	**0.21****	**−0.18***	**−0.17***	ns	**−0.23****	**−0.18***	ns	ns	ns	ns
DLT3	log(C)	ns	ns	**0.32**†	**0.46**†	ns	ns	ns	**0.18***	**0.16***	ns	ns	**−0.50**†	**−0.17***	**0.16***	**−0.32**†	ns	ns	**0.15***	ns	ns	ns	ns
	log(Load)	ns	ns	**0.31**†	**0.46**†	ns	ns	ns	**0.20****	**0.18***	ns	ns	**−0.50**†	**−0.18***	**0.19****	**−0.31**†	ns	ns	**0.16***	**0.15***	ns	ns	ns
DLT4	log(C)	ns	ns	**0.30**†	**0.44**†	**−0.16***	ns	ns	**0.16***	ns	ns	**−0.19****	**−0.50**†	**0.15***	ns	**−0.35**†	**−0.18***	ns	ns	ns	ns	**−0.17***	ns
	log(Load)	ns	ns	**0.27**†	**0.45**†	ns	ns	ns	**0.16***	**0.15***	ns	ns	**−0.50**†	**0.15***	ns	**−0.35**†	ns	ns	**0.15***	ns	ns	ns	ns

C: concentration; Q: discharge; S: storage; P: rainfall; DS: downslope; MS: midslope; US: upslope; ns: not significant.
* Significant at 0.05.
** Significant at 0.01.
† Significant at 0.001.

3.3. Timing of tracer breakthrough and hydrologic variable peaks

All hydrologic variables (discharge, storage, water level at three locations (downslope, midslope and upslope), and a total of 15 volumetric water contents at three locations (downslope, midslope and upslope) and 5 depths (5, 20, 35, 50, 85 cm) were sorted based on the time at which each variable peaked in response to the rainfall pulse (Table 4). Rainfall was the main driver of the hydrologic response in the periodic, steady state system. In response to rainfall, the mid-slope VWC at 35 cm depth peaked first on most days, supporting the hypothesis of a potential preferential flowpath created by the dripping water from the beam over the lysimeter (Fig. 1b). Storage always peaked at the end of each corresponding rainfall pulse and during most days, storage was the 7th variable to peak, preceded by peaks in VWC in the near surface (5 and 20 cm depth) of the lysimeter. All variables that peaked before storage were defined as quick response variables (shaded blue in Table 4).

Discharge often occurred as 10th to 13th peak among all hydrologic variables. Based on the arrival of the discharge peak, variables that peaked between storage and discharge were defined as medium response variables. Finally, variables that peaked after discharge were defined as slow response variables. In general, the VWC at shallow depth peaked earlier than the VWC at deeper depth irrespective of the slope position. In terms of lateral water movement, VWC at the same depth in the downslope position generally peaked before the upslope position (Table 4). During all rainfall pulses, the water level in the upslope position always peaked before the upslope VWC at 85 cm depth: the upslope VWC at 85 cm depth almost always ranked 20, while the upslope water table ranked between 14 and 19 (Table 4). This indicated that lateral flow in upslope direction, instead of vertical infiltration, contributed significantly to upslope water table rise. Otherwise, i.e., if the vertical infiltration were the main contribution to upslope water table rise, the upslope water table should rank after the upslope VWC at 85 cm. A similar behavior was observed for the midslope and downslope positions, but only during the third rainfall pulse on each day, when the mid-slope and downslope water table rose quickly in response to the combined effect of vertical and lateral flow. At all other times, the VWC at 85 cm peaked before the water level at the mid-slope and downslope position.

The repetitive daily pattern in VWC, water level, discharge and storage dynamics are of fundamental importance for the transport of the DLTs and D in the system as discussed in more detail below. In response to precipitation inputs and the hydrologic response of the system, different DLT transport hotspots emerged over the course of each day during the 10-day experiment. In the morning (8:00–12:00), rainwater infiltrating into the unsaturated zone created a flow and tracer transport hotspot that caused movement of some of the DLT particles deeper into the system; in the afternoon (12:30–20:30), both the unsaturated and variably saturated zone influenced flow and tracer transport; while, at night (21:00–7:30 of next day), the variably saturated zone was driving most of the tracer transport (see hydrologic parameter analysis provided in Table 4). The main drivers of the D peaks were percolation of the infiltrating rainwater through the unsaturated zone, subsequent water table rise in the upslope, mid-slope and downslope bottom part of the hillslope, and eventual increase in discharge and soil moisture at the location closest to the outlet (Table 4). These dynamics in combination with the rainfall pulses were also the main drivers of the DLT peaks. However, most of the time more than one driver was taking effect.

3.4. Soil retention and recovery rates

All four particle tracers (DLTs) showed an exponential decline in retained tracer percentage with depth (Table 2, soil zones). More than 90% of the applied tracer mass was retained in the first 5 cm of the porous media (Table 2, soil zone 0–5 cm), which was consistent with

Table 4
Hydrologic variables ranked for each rainfall pulse and day based on the arrival time of the variable's peak. The color of each cell indicates the response time category: blue cells indicate quick response variables and storage, green cells indicate medium response variables and discharge, and grey cells indicate slow response variables slower than storage and discharge peak.

		DAY 1						DAY 2						DAY 3					
		VWC					WL	VWC					WL	VWC					WL
		5	20	35	50	85		5	20	35	50	85		5	20	35	50	85	
Peak 1	US	5	7	10	16	20	19	5	8	10	16	20	19	6	8	10	15	20	18
	MS	2	4	2	14	15	18	3	4	1	12	15	17	3	4	1	13	13	16
	DS	1	6	9	11	13	17	2	6	9	11	14	17	2	5	9	11	19	17
	S	7						7						7					
	Q	12						12						12					
Peak 2	US	6	8	10	14	20	19	6	7	10	14	20	19	6	7	10	14	20	19
	MS	3	4	1	12	14	18	4	5	1	12	15	16	4	3	1	12	15	18
	DS	2	5	9	10	17	16	2	3	9	11	18	17	2	5	9	11	16	17
	S	7						7						7					
	Q	13						13						13					
Peak 3	US	6	8	11	16	20	15	6	7	12	16	20	15	6	7	11	15	20	14
	MS	3	4	1	12	19	14	3	5	1	14	19	13	2	4	1	12	19	18
	DS	2	4	10	9	18	17	2	3	10	9	18	17	3	5	9	10	17	16
	S	7						7						8					
	Q	13						11						13					

		DAY 4						DAY 5						DAY 6					
		VWC					WL	VWC					WL	VWC					WL
		5	20	35	50	85		5	20	35	50	85		5	20	35	50	85	
Peak 1	US	5	8	10	16	20	19	6	8	10	16	20	17	6	8	10	16	20	19
	MS	3	4	1	12	14	18	3	4	1	13	15	19	3	5	1	13	15	17
	DS	2	5	9	11	15	17	2	5	9	11	14	18	2	4	9	11	14	18
	S	7						7						7					
	Q	12						12						12					
Peak 2	US	5	9	11	15	20	19	6	8	10	14	20	19	6	9	10	14	20	17
	MS	3	5	1	12	14	17	4	4	1	13	15	18	3	4	1	12	15	18
	DS	2	3	10	8	16	18	2	3	9	11	16	17	2	5	7	11	15	19
	S	7						7						7					
	Q	13						12						13					
Peak 3	US	6	8	11	15	20	14	5	8	11	17	20	15	6	8	11	17	19	15
	MS	3	5	1	12	19	16	3	4	1	12	19	14	3	5	1	13	20	14
	DS	2	4	9	10	18	17	2	5	9	12	18	16	2	4	9	10	18	16
	S	7						7						7					
	Q	12						10						11					

		DAY 7						DAY 8						DAY 9					
		VWC					WL	VWC					WL	VWC					WL
		5	20	35	50	85		5	20	35	50	85		5	20	35	50	85	
Peak 1	US	6	8	10	16	20	18	5	8	10	16	20	19	6	8	10	16	20	19
	MS	3	4	1	13	15	17	3	6	1	13	15	18	3	4	1	13	15	18
	DS	1	5	9	11	14	19	2	4	9	11	14	17	2	5	9	11	14	17
	S	7						7						7					
	Q	12						12						12					
Peak 2	US	6	7	10	14	20	17	6	7	10	14	20	19	6	8	10	14	20	19
	MS	3	4	1	11	15	19	5	4	3	12	17	18	3	5	1	13	15	17
	DS	2	5	9	11	16	18	1	2	9	11	15	16	2	4	9	11	16	18
	S	7						7						7					
	Q	11						12						12					
Peak 3	US	6	7	12	16	17	15	6	7	11	18	20	16	6	9	11	16	19	15
	MS	1	4	1	13	19	14	3	3	2	13	16	13	3	5	1	12	20	14
	DS	3	4	9	9	20	18	1	5	7	10	19	15	2	4	7	12	18	17
	S	7						7						7					
	Q	11						11						10					

		DAY 10					
		VWC					WL
		5	20	35	50	85	
Peak 1	US	5	8	10	16	20	19
	MS	3	4	1	12	15	17
	DS	2	6	9	11	14	18
	S	7					
	Q	13					
Peak 2	US	6	7	10	16	20	15
	MS	2	4	1	12	17	14
	DS	3	4	9	11	18	19
	S	8					
	Q	13					
Peak 3	US	6	7	12	16	20	15
	MS	3	4	1	13	19	14
	DS	2	5	9	10	17	18
	S	8					
	Q	11					

Q: discharge; S: storage; DS: downslope; MS: midslope; US: upslope; VWC: volumetric water content (the 5, 20, 35, 50 and 85 refer to measurement depth); WL: water level.

the significant correlation between the VWC at 5 cm and DLT breakthrough mentioned at the end of Section 3.2.2. On average 5.2% was retained in the 5–50 cm zone of the soil, while only trace amounts (on average $< 0.2\%$) were observed in the lower half (50–100 cm) of the soil lysimeter (Fig. 7 and Table 2). For all DLTs, less than 1.5% of the applied mass passed through the unsaturated zone (0–50 cm); however, except for DLT3, once particles could enter the variably saturated zone (lower 27 cm of the lysimeter), more than 99% (if not 100%) went into discharge and were exported from the system (Fig. 7 and Table 2). Recall again that the perfect mass balance was due to the way we estimate the total input DNA copies (Eq. (5)).

On average only about 0.86% of the applied DLT mass moved through the unsaturated zone and reached the fluctuating water table (Table 2, summation of total discharge and soil zone 50–100 cm percentage). This low mass recovery is consistent with the very low biocolloid recovery observed by Auset et al. (2005) in an unsaturated soil column experiment with transient flow pulses. Toran and Palumbo (1992) observed less than 1% recovery of 1 μm microspheres in a 65 cm saturated repacked sand column, which is comparable to the percentage that was recovered in this experiment even though the lysimeter had a 75 cm unsaturated and a 25 cm variably saturated zone.

4. Discussion

4.1. Five unique characteristics of the DLT breakthrough curves and the speculated reasons

The synchronous and sequential application of four DLTs in this periodic, steady state flow and transport experiment point towards some interesting mechanisms that were, to our knowledge, not studied in combination in previous experiments so far:

4.1.1. Decreasing DLT recovery for sequentially applied tracers

Although the size and zeta potential of the monodispersed DLTs were similar (Table 1), DLT1, DLT2 and DLT3, which were applied during the first, second and third rainfall events, respectively, on the

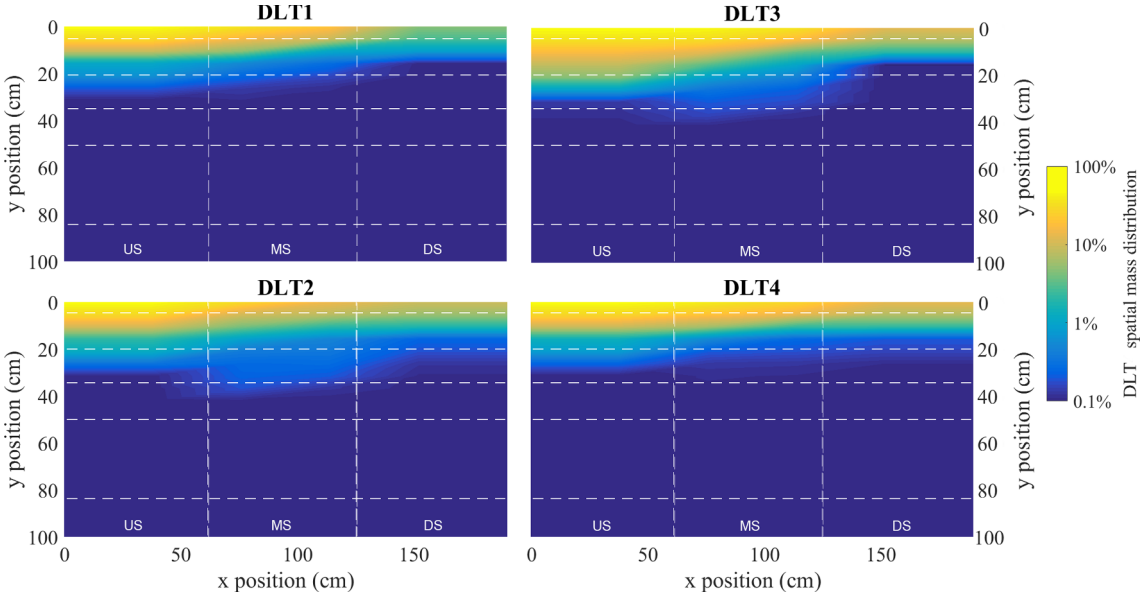

Fig. 7. Spatial distribution of particle tracer mass retained by the porous media at the end of the 10-day experiment for each DLT. White dashed lines show the 18 zones from which soil samples were taken. US, MS, and DS indicate the upslope, midslope and downslope position.

first day of the experiment, showed a consistently decreasing recovery rate (Table 2, total discharge percentage). We speculate that one mechanism that could account for this is the sequentially increasing retention due to the clogging of pore throats by the DLTs. This would progressively increase straining of the DLTs over time. This mechanism has been observed directly in other studies (Auset and Keller, 2006; Bradford et al., 2006; Xu et al., 2006). DLT1 showed the greatest recovery in discharge (Table 2, 1.44% in discharge). This might be attributable to the fact that DLT1 was applied first, when no other tracers blocked its pathways. DLT4 was applied at the same time as DLT1, but the concentration was 1/3 of that of DLT1, and its second and third pulses were applied after DLT1. Since the tracer application during the first rainfall event on Day 1 was not blocked by other tracers but the second and third pulses might have been, the DLT4 recovered mass turned out to be the second highest (Table 2, 1.04% in discharge). DLT2 was applied during the second rainfall pulse (Fig. 5) when the lysimeter was wetting up and hydrologic connectivity was established between the unsaturated and permanently saturated zone. Nearly 70% of DLT2 was transferred within the same rainfall pulse (Fig. 6, day 1 pulse 2). This seems to suggest that the majority of the recovered DLT2 particles might have found rapid transport pathways during its application which were blocked during subsequent events, either by previously added tracers or by air bubbles, resulting in the second lowest recovery rate (Table 2, 0.52% in discharge). DLT3 was applied during the third rainfall event on day 1 after which it experienced a 14 h long drying period (Fig. 5). The lack of rainfall might have caused DLT3 particles to become quickly trapped by physico-chemical adsorption or straining, which resulted in the lowest recovery rate (Table 2, 0.19% in discharge).

4.1.2. Highly variable number of peaks

As shown in Fig. 5, each DLT breakthrough curve exhibited several, and often with inconsistent timing, high-concentration peaks (i.e. high DNA-copy count per sample) throughout the experiment. We hypothesize that the main reason for this erratic breakthrough was the intermittent wetting-drying cycle created by the periodic rainfall events. The low soil water content between rain events hindered the movement of particles, as particles must move with the water flow (Fig. 5). This dynamic was further exacerbated by the size and mass of the particles, and their potential aggregation over time (Fig. 2), which increased the probability of particle retention in the porous media while at the same time increasing the probability for spontaneous dislodging and transport through the system during rainfall events (Auset et al., 2005; Zhuang et al., 2007). Theoretically, if the system were to remain saturated throughout the experiment, then based on the ratio of the porous media diameter, d_m, to the DLT particle diameter, d_p (d_m/d_p) (Fig. 2), most particles should have be retained in the near surface soil layer by physical-chemical filtration (more than 90% of the porous media had a $d_m/d_p > 20$, Fig. 2), i.e. collision with and attachment to soil-water interfaces (McDowell-Boyer et al., 1986). However, actually, due to the unsaturated condition, the proportion of DLTs subject to physical-chemical filtration should be less than the calculated value; and proportion of straining (e.g. wedging, bridging, retention at solid-air-water triple point, or film straining in water films enveloping the solid phase) and attachment of DLTs to air-water interfaces should be greater than the calculated value for straining (Bradford and Torkzaban, 2008). Cake filtration was unlikely, both theoretically and actually, since only 2.4% of the porous media had a $d_m/d_p < 10$ (Fig. 2), and this proportion would not be influenced by the saturation condition.

4.1.3. Faster DLT transport than D at the beginning of experiment, but exceeded by D soon after the start of D breakthrough

DLT1, DLT2 and DLT4 showed a faster breakthrough than was observed for the deuterium at the beginning of the experiment (before the end of the third rainfall pulse on Day 1 of experiment, Figs. 5 and 6). We hypothesize that the faster breakthrough at the beginning can be attributed to 1) the formation of a capillary barrier (Bussière et al., 2003; Predelus et al., 2015; Walter et al., 2000) at the interface between the finer textured soil matrix and the gravel layer near the downslope face of the lysimeter, which facilitated preferential flow of water and DLT particles and 2) the size exclusion effect.

A capillary barrier is often formed under unsaturated conditions at the interface of a finer-textured and a coarser-textured soil when the water pressure at the interface cannot reach the water entry pressure of the coarser-textured soil. Water is held in the finer-textured soil by capillary force effectively preventing water from entering the coarser-textured soil (Bussière et al., 2003; Walter et al., 2000). As a result, the interface acts as preferential flow pathway (Bussière et al., 2003; Walter et al., 2000), facilitating fast solute and colloid transport (Predelus et al., 2015). A capillary barrier likely formed at the 80-degree interface between the soil and the gravel in the sloped lysimeter. Since the gravel layer had nearly no suction pressure, preferential flow formed along the interface in the unsaturated zone allowing tracers that were applied close to the capillary barrier to travel much faster than the D front which was the weighted average of the fast water flow at the capillary barrier and the much larger amount of slow water flow in the soil matrix.

Size exclusion happens when some of the pores in the systems are not hydrodynamically accessible to the particle (Bradford and Torkzaban, 2008; Sirivithayapakorn and Keller, 2003a). Particles are excluded from the pores that do not have enough liquid to move them through (Bradford and Torkzaban, 2008). Even if the system is saturated, particles tend to choose broader pathways over narrower ones (Sirivithayapakorn and Keller, 2003a) and tend to travel near the center of pores where velocity is larger (Sirivithayapakorn and Keller, 2003a). We speculate that due to the size exclusion effect, the 1-μm DLT particles were constrained to connected larger pores filled with enough water resulting in faster transport of DLT particles than the bulk water and D front (Figs. 5 and 6) at the beginning.

D started to breakthrough around the beginning of the third rain pulse on the first day and the normalized cumulative transferred mass exceeded the DLTs within 2.5 h (Fig. 6b). This was due to the strong straining of the DLTs by the soil matrix and the strong physical-chemical adsorption of the DLTs to the soil matrix. The retention effects of these two mechanisms together were about two orders of magnitude stronger than the mobilization effect of preferential flow in our system for the 1-μm DLT particles (comparing the about 1% recovery rate of the DLTs with the 97.78% recovery rate of D).

4.1.4. Lack of coincidence between DLT peaks and discharge peaks

Contrary to Auset et al. (2005) whose colloid breakthrough peaks were coincident with discharge peaks, most of our DLT breakthrough peaks occurred during and right after the rainfall events (Fig. 5, Table 4) but often before the corresponding discharge peaks (Fig. 3). We hypothesize that this difference was caused by the nature of the soil system. In Auset et al.'s (2005) vertical soil column experiments, the discharge was collected at the bottom of the columns, which means that the colloids had to move through the entire column and travel the same length as water to reach the outlet. However, in our sloped soil lysimeter, as discussed above in Section 4.1 *iii)*, significant amount of DLTs that were able to get discharged moved along the fast pass—capillary barrier, which was shorter than average pathway of water flow. Hence, in contrast to other studies that observed synchronous colloid breakthrough and discharge peaks, our colloid breakthrough peaks occurred earlier than the corresponding discharge peaks.

4.1.5. Abnormally high, late DLT peaks

Contrary to the results of Auset et al. (2005) who showed that after the second peak, the height of the peaks were consistently decreasing over time, we observed some peaks later during the experiment, which had DNA copy counts similar to some of the earlier peaks (Fig. 5, DLT3

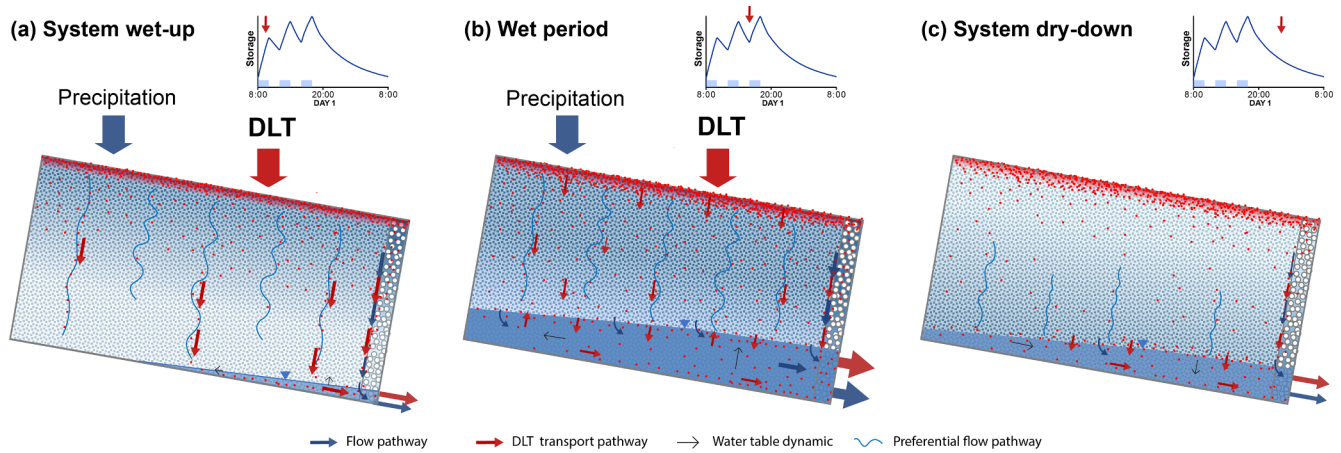

Fig. 8. Schematic of hypothesized DNA-labelled particle tracer (DLT) transport pathways in the sloped lysimeter under different wetness conditions. (a) During system wet-up, when rainfall and DLT tracers are applied, a wetting front is progressing into the system. DLTs could be transported along preferential flow pathways and the capillary barrier near the downslope face of the system. (b) At the peak of the wet period, the wetting front reached the bottom of the system, the water table is rising and mobile tracers entering the saturated zone could be transported out of the system. (c) At the beginning of the dry period, larger discharge and a faster drying front could mobilize DLT particles from the variably saturated zone, leading to DLT peaks after midnight.

and DLT4).

We hypothesize that this was due to cluster/flocculation/aggregate formation of the DLT particles in the soil system. The tracer solutions were monodispersed and stable (in ultrapure water) when they were applied onto the system, since they were well mixed and the zeta potential of the DLTs was within the range of moderate stability (−30–40 mV). However, once the particles arrived at the unsaturated soil surface, there were several mechanisms that might have caused aggregation. First, surface filtered particles might have formed a cake on the soil surface (Auset and Keller, 2006; Mackley and Sherman, 1992), and some aggregates from the cake might have found their way into the soil system when raindrops disturbed the soil surface and changed the pore structures in top soil (e.g. breaking of the cake into smaller clusters) (Wang et al., 2013). Second, the particles that were attached to the air-water interface could form a cluster when the AWI gradually shrank and finally dissolved during imbibition (see Fig. 3 of Sirivithayapakorn and Keller (2003b) for the visualization of this cluster formation process). Third, the particles deposited at the same spot on a soil grain could form a cluster (see Fig. 11 of Keller and Auset (2007) for the visualization of this cluster formation process). When some driver(s) mobilized the clusters, high colloid loads would occur in the seepage samples.

Further, the periodic, steady state condition of the experiment created a fluctuating water table and capillary fringe that changed position in both the vertical and horizontal direction. The fluctuating capillary fringe could largely help in mobilizing colloids both when the capillary fringe was rising and falling (detailed description of possible colloid mobilization by fluctuating capillary fringe is given in Section 4.2).

4.2. Conceptualization of hypothesized transport processes in a dynamic and complex system

4.2.1. System wet-up

When it started to rain at 8:00 on each day (Fig. 8a), the impact of the raindrops might have enabled redistribution of soil and tracer particles in the top one centimeter of the soil (similar to the shield layer or mixing layer in Wang et al., 2013, 2017, 2018). As a result, tracers in the top 1 cm of soil might have been ejected and deposited into larger pores allowing them to move more deeply in the soil.

Once DLT particles were deposited into larger pores, a series of processes could enable their transport to the variably saturated zone and the outlet of the lysimeter. During the first rainfall pulse each day (Fig. 8a), the infiltrating rainwater created a wetting front that moved downwards. Air-filled pores increasingly filled with water as the wetting front was passing, creating a thicker water film around soil grains. As a result, the location of AWIs was moving and the total area of AWIs was getting smaller (Auset et al., 2005). The increase in water content might have also caused a disturbance of the hydrostatic equilibrium formed at SWI(s) or solid-air-water triple points (Lazouskaya et al., 2013; Zhuang et al., 2007), leading to the mobilization and transport of strained tracers with the wetting front (Lazouskaya et al., 2013).

Besides this series of processes, DLT particles dislodged by raindrops could have entered preferential pathways (along the capillary barrier at the loamy sand and gravel interface or through connected large pores filled with enough water) to reach the outlet faster than the water front (see small red arrows in Fig. 8a). Dislodging might have also allowed retained particles to re-enter flow and transport pathways in the system, leading to successive transport further down in the system. We could not determine whether the dislodged particles were exactly the same ones recovered in discharge shortly after, but dislodging is one of the processes hypothesized that ensured particle tracer mass was mobile within the system, which might eventually exit the system and contribute to the late peaks observed in the DLT breakthrough curves (Fig. 5).

4.2.2. Wet period

When the wetting front reached the bottom of the lysimeter and connected with the capillary fringe (Fig. 8b), the mobile tracers could have entered the saturated zone, which started to expand in the upslope and vertical direction in response to the rainfall input. As the capillary fringe was rising, more and more mobile tracers, as well as immobile tracers strained in the variably saturated zone could have been flushed towards the outlet or seepage face. This mobilization of DLT particles by the rising capillary fringe could explain the tracer peaks that often occurred during the 1st and 2nd rainfall pulse (Fig. 5). Although this particle mobilizing process was mainly driven by the first rainfall pulse, it lasted until the 2nd rainfall pulse because it took several hours for the wetting front to reach the capillary fringe. When any of the particle mobilizing processes coincided with an increase in discharge, its effectiveness could be enhanced by the increase in discharge and flow velocity, which would have flushed the mobile tracers out of the system (Fig. 8b). During the 2nd rainfall pulse the unsaturated zone was smaller and wetter, and the saturated zone was larger. This allowed faster movement of the wetting front (caused by the 2nd rainfall pulse) through the unsaturated zone and more mobilization of strained DLT particles.

4.2.3. Begin of dry period

The effect of the third rainfall pulse each day was to some extent similar to the 2nd rainfall pulse. However, due to the even wetter antecedent moisture conditions, the water table was higher and the capillary fringe was able to reach retained tracers at higher locations. The higher capillary fringe led also to larger hydrostatic pressure which resulted in larger discharge and a faster drying front after the water table peaked (Fig. 8c). The larger discharge could be more effective at flushing out the tracers because it facilitated a larger hydrodynamic shear. The faster drying front could be very effective at mobilizing tracers after rainfall inputs had ceased. Most of the DLT breakthroughs observed after midnight could be attributed to the mobilization of particles with the drying front.

4.3. Possible limitations and uncertainties in interpreting breakthroughs

Saturated soil column experiments using the same tephra soil were conducted prior to the miniLeo experiment to estimate the DLT mass required for the sloped lysimeter experiment. However, due to the predominantly unsaturated conditions in the lysimeter (which were not anticipated), DLT recovery in discharge was low and most DLT mass was retained in the upper soil layer. This resulted in low DLT concentrations in discharge and discharge samples needed to be concentrated 10 fold to obtain the breakthrough curves (details on the method are provided in supplementary materials "sample preparation for analysis").

Due to unknown losses listed in Section 2.3, we had to use the sum of the discharged mass and the mass retained in soil to serve as the total input DLT mass. The technique has been improved a lot since we did this miniLeo experiment, and now we can 1) fabricate the DLTs with higher encapsulation efficiency and higher stability (mitigating aggregation), and 2) analyze samples with higher extraction efficiency (McNew et al., 2018). Now the actual input should be much closer to the total input calculated by Eq. (2).

There was inevitably some uncertainty related to the measured D and DLT concentrations, as is for any measured data. When calculating the normalized load and normalized cumulative transferred mass, more uncertainty was introduced, as we had to assume that the concentration was constant over a certain sampling interval for load calculation, which, because of the high variability in DLT concentrations, might have introduced some uncertainty into the estimated total recovered mass. In addition, for the mass calculation we had to assume that the concentration changed linearly from one to the next sampling point. Some of this uncertainty could be potentially reduced or quantified by a higher sampling frequency. However, for this experiment, DLT concentrations were determined as accurate as possible, and the uncertainties should not change the main results that 1) DLT1, DLT2 and DLT4 transferred faster than D at the beginning of the experiment but transferred much slower than D after the breakthrough of D started, and 2) D recovery rate was close to 100%, while DLT recovery rates were very low, but the recovery rate of earlier applied DLT tracers was still larger than that of the later applied DLT tracers.

Some of the tracer dynamics described in Section 4.1 could also have been influenced by subtle changes in the soil system itself. Although we cannot exactly quantify these changes, there were several pointers in the hydrometric data that indicate that the porous media in the lysimeter was changing over time, possibly as the result of fine sediment particle transport within the system. And the mobilization of fine sediments by unsaturated transient flow was recorded in previous studies, for example, Zhuang et al. (2007). Hence, over time, fewer fine sediment particles remained in the top layer of soil, which might explain why DLT3 had the largest percentage of tracer mass passing through the top 0–5 cm layer (11.8%), while the percentage of the DLT3 mass recovered in the discharge was the smallest (0.19%) (Table 2) (Harvey et al., 1993).

Ionic strength and pH are known to have fundamental controls on physical-chemical adsorption and colloid transport. Although the ionic strength and pH of the seepage water were changing over the course of the experiment (data not shown), the effect of ionic strength on DLT transport was not our main focus in this experiment. Ionic strength of the seepage water varied between 2.56 and 4.51 mmol/L during the experiment, which is almost negligible compared to studies that focused on the role of ionic strength in colloid transport (Auset and Keller, 2006; McDowell-Boyer et al., 1986; Sang et al., 2013; Wan and Wilson, 1994b; Zhuang et al., 2007). The ionic strength observed during this experiment is in the low range (Auset and Keller, 2006; McDowell-Boyer et al., 1986; Sang et al., 2013; Wan and Wilson, 1994b; Zhuang et al., 2007); therefore, it should have played a minor role in the attachment of DLT particles to AWI or SWI or the aggregation of colloids.

4.4. Implications for understanding complex or large scale hydrological systems

The broader novelty of this research is that the use of multiple, unique DLTs opens new avenues for the study of dynamic, complex or large scale hydrological flow and pollutant transport systems, such as flow through glaciers, karst groundwater, flashy arid watersheds, and fill-spill dynamics (Bakalowicz, 2005; Fountain et al., 2005; Fountain and Walder, 1998; Pilgrim et al., 1988; Shaw et al., 2012). As such, this experiment highlights the versatile applicability of DLTs in column to hillslope scale experiments that could potentially provide new insights into the dynamic transport and interaction of, for example, earlier applied and later applied colloidal tracers or synchronously applied tracers at different injection locations, which thus far has not been possible for colloid tracers of the same type, due to the system memory effect (when using the same tracer) (Falbo et al., 2013; Kim et al., 2016). For example, Falbo et al. (2013) measured the overall *Escherichia coli* concentration in a ditch (Fig. 2 in Falbo et al., 2013), which was the result of two near-by manure-application events. However, because the *Escherichia coli* strain they studied had only one unique ID they were not able to quantify the contribution from either event to the total concentration observed. In another example, Kim et al. (2016) repeatedly applied the same tracer (chloride) to a soil lysimeter system and, as a result, a significant lag was required after each application to ensure there was no significant interference between breakthrough signals. Post-processing was also required to decouple the overlap that did occur between breakthroughs. The DLT technology applied in this study facilitates explicit mapping of different source locations and injection times, if a unique DLT were applied during each event. In this manner, DLTs could aid water quality and ecological research through system-specific quantification of transport, diffusion, mechanic dispersion, interception, sedimentation, and filtration of the tracer in the system (Bradford et al., 2003; Yao et al., 1971), and hence prediction of non-point source and point-source particulate pollutants at the catchment scale. The information gained from individual DNA-labelled traces could also improve flow and transport modeling, since changes in the transport dynamics over time can be more accurately captured. This experiment and tracer technology therefore highlight first steps towards improved understanding of the fate and transport of repeated pollution events, such as pathogen pollution from manure applications, by observing the breakthrough of repeated uniquely labelled particle tracer injections under controlled laboratory settings that simulate the dynamics found in many natural hydrologic systems.

5. Conclusions

We applied four unique DNA-labelled particle tracers (DLTs) and one conservative tracer (D) during three 2-hour rainfall events on a sloped, homogeneous soil lysimeter to gain insights into the transport processes of earlier and later applied particle tracers over 10 days of dynamic and transient flows. The results from this experiment highlighted several interesting mechanisms that can inform understanding

of colloid transport processes in the environment such as the transport of colloidal pathogens (e.g. *Salmonella enterica*, *Escherichia coli*) from repeated manure applications in agricultural landscapes. In our experiment, DLTs showed faster early breakthroughs than the conservative D, but were exceeded soon after the start of D breakthrough. DLT breakthroughs were characterized by several, and often with inconsistent timing, high-concentration peaks early in the 10-day experiment followed by erratic high-concentration peaks later in the experiment that did not coincide with discharge peaks. DLT recovery overall was low (< 1.5% of applied mass) and decreased for each subsequently applied tracer. The DLT breakthrough curves can be explained by the intermittent wetting-drying cycle created by the periodic rainfall events, which controlled the volumetric soil water content, water table height and velocity distribution within the soil lysimeter and as such the movement via preferential flow (caused by capillary barrier or size exclusion effect) and retention in the soil matrix. The majority of the applied DLTs were retained near the soil surface either by physical-chemical filtration due to the more than 20 d_m/d_p, or by some kind of straining due to the unsaturated condition. Results from this study were consistent with many colloid transport studies in saturated and unsaturated porous media but some of the breakthrough patterns were unique and warrant additional research to explain the controlling processes, e.g., potential interactions between earlier and later applied DLTs. Future research will focus on 1) modeling the transport processes of multiple DLTs in transient flow systems; 2) applying a mixture of variably sized and labelled DLTs to better understand the size exclusion effect; 3) conducting similar experiments at larger scales (e.g. hillslope) to better understand the processes in natural conditions.

Declaration of interests

The authors declare that they have no known competing financial interests or personal relationships that could have appeared to influence the work reported in this paper.

Acknowledgement

This work was supported by the Heising-Simons Foundation [grant #2014-59], an Axel Wenner-Grens Stiftelse sabbatsstipendium and the Baltic Sea Center and Baltic Nest Institute at Stockholm University. The authors would like to thank the STAR students at the University of Arizona for their support and help at Biosphere 2. The authors would also like to thank Seanna McLaughlin and Brett Bemowski for their help on fabricating and analyzing the DLTs.

Appendix A. Supplementary data

Supplementary data to this article can be found online at https://doi.org/10.1016/j.jhydrol.2018.11.050.

References

Artinger, R., et al., 2002. Humic colloid-borne migration of uranium in sand columns. J. Contam. Hydrol. 58 (1–2), 1–12. https://doi.org/10.1016/S0169-7722(02)00032-3.
Auset, M., Keller, A.A., 2006. Pore-scale visualization of colloid straining and filtration in saturated porous media using micromodels. Water Resour. Res. 42 (12).
Auset, M., Keller, A.A., Brissaud, F., Lazarova, V., 2005. Intermittent filtration of bacteria and colloids in porous media. Water Resour. Res. 41 (9).
Bakalowicz, M., 2005. Karst groundwater: a challenge for new resources. Hydrogeol. J. 13 (1), 148–160.
Barton, C.D., Karathanasis, A.D., 2003. Influence of soil colloids on the migration of atrazine and zinc through large soil monoliths. Water Air Soil Pollut. 143 (1–4), 3–21. https://doi.org/10.1023/A:1022886225564.
Bradford, S.A., Simunek, J., Bettahar, M., Van Genuchten, M.T., Yates, S., 2006. Significance of straining in colloid deposition: evidence and implications. Water Resour. Res. 42 (12).
Bradford, S.A., Simunek, J., Bettahar, M., van Genuchten, M.T., Yates, S.R., 2003. Modeling colloid attachment, straining, and exclusion in saturated porous media. Environ. Sci. Technol. 37 (10), 2242–2250.
Bradford, S.A., Torkzaban, S., 2008. Colloid transport and retention in unsaturated porous media: A review of interface-, collector-, and pore-scale processes and models. Vadose Zone J. 7 (2), 667–681.
Bradford, S.A., Torkzaban, S., Leij, F., Šimůnek, J., van Genuchten, M.T., 2009. Modeling the coupled effects of pore space geometry and velocity on colloid transport and retention. Water Resour. Res. 45 (2). https://doi.org/10.1029/2008WR007096.
Bradford, S.A., Yates, S.R., Bettahar, M., Simunek, J., 2002. Physical factors affecting the transport and fate of colloids in saturated porous media. Water Resour. Res. 38 (12).
Bussière, B., Apithy, S.A., Aubertin, M., Chapuis, R.P., 2003. Water diversion capacity of inclined capillary barriers, Canadian Geotechnical Conference, Winnipeg, Manitoba, Canada.
Chrysikopoulos, C.V., Sim, Y., 1996. One-dimensional virus transport in homogeneous porous media with time-dependent distribution coefficient. J. Hydrol. 185 (1–4), 199–219.
Crist, J.T., et al., 2004. Pore-scale visualization of colloid transport and retention in partly saturated porous media. Vadose Zone J. 3 (2), 444–450.
Dahlke, H.E., et al., 2015. Using concurrent DNA tracer injections to infer glacial flow pathways. Hydrol. Process. 29 (25), 5257–5274.
de Jonge, L.W., Moldrup, P., Rubæk, G.H., Schelde, K., Djurhuus, J., 2004. Particle leaching and particle-facilitated transport of phosphorus at field scale. Vadose Zone J. 3 (2), 462–470. https://doi.org/10.2136/vzj2004.0462.
M. Elimelech J. Gregory X. Jia 2013. Particle Deposition and Aggregation: Measurement, Modelling and Simulation. Butterworth-Heinemann.
Falbo, K., et al., 2013. Roadside ditches as conduits of fecal indicator organisms and sediment: implications for water quality management. J. Environ. Manage. 128, 1050–1059.
Flury, M., Wai, N.N., 2003. Dyes as tracers for vadose zone hydrology. Rev. Geophys. 41 (1).
Fountain, A.G., Jacobel, R.W., Schlichting, R., Jansson, P., 2005. Fractures as the main pathways of water flow in temperate glaciers. Nature 433 (7026), 618–621.
Fountain, A.G., Walder, J.S., 1998. Water flow through temperate glaciers. Rev. Geophys. 36 (3), 299–328.
Gevaert, A., et al., 2014. Hillslope-scale experiment demonstrates the role of convergence during two-step saturation. Hydrol. Earth Syst. Sci. 18 (9), 3681.
Goldberg, E., et al., 2017. What factors determine the retention behavior of engineered nanomaterials in saturated porous media? Environ. Sci. Technol. 51 (5), 2729–2737.
Gómez Suárez, C., Noordmans, J., Van der Mei, H., Busscher, H., 1999. Removal of colloidal particles from quartz collector surfaces as stimulated by the passage of liquid-air interfaces. Langmuir 15 (15), 5123–5127.
Harvey, R.W., Kinner, N.E., MacDonald, D., Metge, D.W., Bunn, A., 1993. Role of physical heterogeneity in the interpretation of small-scale laboratory and field observations of bacteria, microbial-sized microsphere, and bromide transport through aquifer sediments. Water Resour. Res. 29 (8), 2713–2721.
Keller, A.A., Auset, M., 2007. A review of visualization techniques of biocolloid transport processes at the pore scale under saturated and unsaturated conditions. Adv. Water Resour. 30 (6), 1392–1407.
Kim, M., et al., 2016. Transit time distributions and StorAge Selection functions in a sloping soil lysimeter with time-varying flow paths: direct observation of internal and external transport variability. Water Resour. Res. 52 (9), 7105–7129.
Kretzschmar, R., Borkovec, M., Grolimund, D., Elimelech, M., 1999. Mobile subsurface colloids and their role in contaminant transport. Adv. Agron. 66, 121–193.
Lazouskaya, V., Jin, Y., 2008. Colloid retention at air-water interface in a capillary channel. Colloids Surf. A: Physicochem. Eng. Asp. 325 (3), 141–151.
Lazouskaya, V., Jin, Y., Or, D., 2006. Interfacial interactions and colloid retention under steady flows in a capillary channel. J. Colloid Interface Sci. 303 (1), 171–184.
Lazouskaya, V., et al., 2013. Colloid mobilization by fluid displacement fronts in channels. J. Colloid Interface Sci. 406, 44–50.
Mackley, M., Sherman, N., 1992. Cross-flow cake filtration mechanisms and kinetics. Chem. Eng. Sci. 47 (12), 3067–3084.
McCarthy, J.F., McKay, L.D., Bruner, D.D., 2002. Influence of ionic strength and cation charge on transport of colloidal particles in fractured shale saprolite. Environ. Sci. Technol. 36 (17), 3735–3743.
McDowell-Boyer, L.M., Hunt, J.R., Sitar, N., 1986. Particle transport through porous media. Water Resour. Res. 22 (13), 1901–1921.
McNew, C.P., Wang, C., Walter, M.T., Dahlke, H.E., 2018. Fabrication, detection, and analysis of DNA-labeled PLGA particles for environmental transport studies. J. Colloid Interface Sci. 526, 207–219.
Mills, W.B., Liu, S., Fong, F.K., 1991. Literature-review and model (comet) for colloid metals transport in porous-media. Ground Water 29 (2), 199–208. https://doi.org/10.1111/j.1745-6584.1991.tb00511.x.
Mishurov, M., Yakirevich, A., Weisbrod, N., 2008. Colloid transport in a heterogeneous partially saturated sand column. Environ. Sci. Technol. 42 (4), 1066–1071.
Mohanram, A., et al., 2010. Comparison of transport and attachment behaviors of Cryptosporidium parvum oocysts and oocyst-sized microspheres being advected through three minerologically different granular porous media. Water Res. 44 (18), 5334–5344.
Ouyang, Y., Shinde, D., Mansell, R.S., Harris, W., 1996. Colloid-enhanced transport of chemicals in subsurface environments: a review. Crit. Rev. Environ. Sci. Technol. 26 (2), 189–204. https://doi.org/10.1080/10643389609388490.
Pangle, L.A., et al., 2015. The Landscape Evolution Observatory: a large-scale controllable infrastructure to study coupled Earth-surface processes. Geomorphology 244, 190–203.
Pilgrim, D., Chapman, T., Doran, D., 1988. Problems of rainfall-runoff modelling in arid and semiarid regions. Hydrol. Sci. J. 33 (4), 379–400.
Pohlmann, M., et al., 2016. Pore water chemistry reveals gradients in mineral

transformation across a model basaltic hillslope. Geochem. Geophys. Geosyst. 17 (6), 2054–2069.
Predelus, D., et al., 2015. Combined effect of capillary barrier and layered slope on water, solute and nanoparticle transfer in an unsaturated soil at lysimeter scale. J. Contam. Hydrol. 181, 69–81. https://doi.org/10.1016/j.jconhyd.2015.06.008.
Sang, W., et al., 2013. Quantification of colloid retention and release by straining and energy minima in variably saturated porous media. Environ. Sci. Technol. 47 (15), 8256–8264.
Severino, G., Cvetkovic, V., Coppola, A., 2007. Spatial moments for colloid-enhanced radionuclide transport in heterogeneous aquifers. Adv. Water Resour. 30 (1), 101–112. https://doi.org/10.1016/j.advwatres.2006.03.001.
Sharma, A.N., Luo, D., Walter, M.T., 2012. Hydrological tracers using nanobiotechnology: proof of concept. Environ. Sci. Technol. 46 (16), 8928–8936.
Shaw, D.A., Vanderkamp, G., Conly, F.M., Pietroniro, A., Martz, L., 2012. The fill–spill hydrology of prairie wetland complexes during drought and deluge. Hydrol. Process. 26 (20), 3147–3156.
Sirivithayapakorn, S., Keller, A., 2003a. Transport of colloids in saturated porous media: a pore-scale observation of the size exclusion effect and colloid acceleration. Water Resour. Res. 39 (4).
Sirivithayapakorn, S., Keller, A., 2003b. Transport of colloids in unsaturated porous media: a pore-scale observation of processes during the dissolution of air-water interface. Water Resour. Res. 39 (12).
Smith, J., et al., 2007. Pore-scale quantification of colloid transport in saturated porous media. Environ. Sci. Technol. 42 (2), 517–523.
Toran, L., Palumbo, A., 1992. Colloid transport through fractured and unfractured laboratory sand columns. J. Contam. Hydrol. 9 (3), 289–303.
van Haren, J., et al., 2017. CO2 diffusion into pore spaces limits weathering rate of an experimental basalt landscape. Geology 45 (3), 203–206.
Vasiliadou, I.A., Chrysikopoulos, C.V., 2011. Cotransport of *Pseudomonas putida* and kaolinite particles through water-saturated columns packed with glass beads. Water Resour. Res. 47 (2), W02543.
Veevaert, J., 2012. Mineralogy Database. Veevaert, John.
Walter, M., et al., 2000. Funneled flow mechanisms in a sloping layered soil: laboratory investigation. Water Resour. Res. 36 (4), 841–849.
Wan, J., Wilson, J.L., 1994a. Colloid transport in unsaturated porous media. Water Resour. Res. 30 (4), 857–864.
Wan, J., Wilson, J.L., 1994b. Visualization of the role of the gas-water interface on the fate and transport of colloids in porous media. Water Resour. Res. 30 (1), 11–23.
Wang, C., et al., 2017. Modeling the release of Escherichia coli from soil into overland flow under raindrop impact. Adv. Water Resour. 106, 144–153. https://doi.org/10.1016/j.advwatres.2016.10.016.
Wang, C., et al., 2018. Release of Escherichia coli under raindrop impact: the role of clay. Adv. Water Resour. 111 (Supplement C), 1–5. https://doi.org/10.1016/j.advwatres.2017.10.028.
Wang, C., Walter, M.T., Parlange, J.-Y., 2013. Modeling simple experiments of biochar erosion from soil. J. Hydrol. 499, 140–145.
Xu, S., Gao, B., Saiers, J.E., 2006. Straining of colloidal particles in saturated porous media. Water Resour. Res. 42 (12).
Yao, K.-M., Habibian, M.T., O'Melia, C.R., 1971. Water and waste water filtration. Concepts and applications. Environ. Sci. Technol. 5 (11), 1105–1112.
Zhang, W., et al., 2010. Transport and retention of biochar particles in porous media: effect of pH, ionic strength, and particle size. Ecohydrology 3 (4), 497–508.
Zhang, W., Tang, X.-Y., Weisbrod, N., Zhao, P., Reid, B.J., 2015. A coupled field study of subsurface fracture flow and colloid transport. J. Hydrol. 524, 476–488. https://doi.org/10.1016/j.jhydrol.2015.03.001.
Zhang, W., et al., 2016. A field study of colloid transport in surface and subsurface flows. J. Hydrol. 542, 101–114. https://doi.org/10.1016/j.jhydrol.2016.08.056.
Zhuang, J., McCarthy, J.F., Tyner, J.S., Perfect, E., Flury, M., 2007. In situ colloid mobilization in Hanford sediments under unsaturated transient flow conditions: effect of irrigation pattern. Environ. Sci. Technol. 41 (9), 3199–3204.